



# A multi-parametric perspective of the North Atlantic eddy-driven jet

David Barriopedro<sup>1</sup> · Blanca Ayarzagüena<sup>2</sup> · Marina García-Burgos<sup>1,2</sup> · Ricardo García-Herrera<sup>1,2</sup>

Received: 8 April 2022 / Accepted: 29 October 2022  
© The Author(s) 2022

## Abstract

The North Atlantic eddy-driven jet (EDJ) is an essential component of the Euro-Atlantic atmospheric circulation. It has been typically described in terms of latitude and intensity but this is not enough to fully characterize its variability and complex EDJ configurations. Here, we present a set of daily parameters of the EDJ based on low-tropospheric zonal wind data for the 1948–2020 period. They describe the intensity, sharpness, location, edges, tilt and other zonal asymmetries of the EDJ, therefore dissecting its structure beyond the latitudinal regimes. This allows for assessments of specific EDJ aspects and a multi-parametric treatment of EDJ configurations in a manageable way. Overall, variations in EDJ parameters reflect distinctive patterns of eddy forcing and wave breaking, with anticyclonic eddies playing a major role in shaping the EDJ structure. A multimodal behavior of the EDJ is only detected in latitude, which largely influences the longitudinal position of the EDJ. Other aspects of the EDJ are less constrained by the latitude and display a variety of configurations. Four multi-parametric states (northern, central, tilted and split EDJs) provide a satisfactory description of recurrent patterns of the EDJ. They participate in meridional migrations of the EDJ, but yield less dramatic transitions than viewed from the latitudinal perspective. Finally, the EDJ parameters help to better understand the EDJ influence on European climate. In many regions, latitude and intensity contain limited information on near-surface anomalies, and their signals can be masked by the additional effect of other EDJ parameters.

**Keywords** Eddy-driven jet · North Atlantic atmospheric circulation · Climate dynamics · Climate variability · Climate change · European climate

## 1 Introduction

Jet streams are a key component of the atmospheric circulation. They are forced by angular momentum transport in the upper branch of the Hadley cell and eddy momentum flux convergence and heat forcing from transient eddies (e.g. Held and Hou 1980; Hoskins et al. 1983). In winter, the North Atlantic (NATL) region exhibits two separate jets: a shallower subtropical jet in the upper troposphere and a deeper mid-latitude eddy-driven jet (EDJ; e.g. Eichelberger and Hartmann 2007; Li and Wettstein 2012). The key role

of transient eddy feedbacks and momentum convergence in maintaining the EDJ has been widely documented (e.g. Hoskins et al. 1983; Lorenz and Hartmann 2003; Gerber and Vallis 2007; Zurita-Gotor et al. 2014).

The NATL EDJ describes the storm-track activity and synoptic conditions of the Euro-Atlantic sector, and its variability is associated with the main extratropical teleconnection patterns, therefore connecting regional climate to the large-scale atmospheric circulation (e.g. Monahan and Fyfe 2006; Strong and Davis 2008; Mellado-Cano et al. 2019). Regional climate anomalies and extreme weather events such as heat waves, cold air outbreaks or droughts are typically related to changes in the EDJ structure (Mahlstein et al. 2012; Santos et al. 2013; García-Herrera et al. 2019; Sousa et al. 2021). Woollings et al. (2010) identified three preferred latitudinal positions of the NATL winter EDJ, corresponding to south (S), north (N) and central (C, or undisturbed) states, which are linked to the negative North Atlantic Oscillation (NAO), and negative and positive phases of the East Atlantic (EA), respectively. The S EDJ regime is also connected with

✉ David Barriopedro  
david.barriopedro@csic.es

<sup>1</sup> Instituto de Geociencias (IGEO), Consejo Superior de Investigaciones Científicas - Universidad Complutense de Madrid (CSIC-UCM), C / Doctor Severo Ochoa 7, Ciudad Universitaria, 28040 Madrid, Spain

<sup>2</sup> Dpto. Física de la Tierra y Astrofísica, Facultad de Ciencias Físicas, Universidad Complutense de Madrid (UCM), Parque de Ciencias, Ciudad Universitaria, 28040 Madrid, Spain

Greenland blocking (e.g. Woollings et al. 2010; Hannachi et al. 2012), whereas N EDJs have been related to Greenland orographic forcing of low-level tip jets (White et al. 2019) and/or the development of subtropical ridges (Woollings et al. 2011).

The three latitudinal regimes also exhibit different persistence, which can dictate some predictability of extratropical synoptic conditions (e.g. Franzke and Woollings 2011; Hannachi et al. 2012; Frame et al. 2013). In particular, N EDJs display lower persistence and forecast skill than the other latitudinal regimes (Frame et al. 2011; Franzke et al. 2011), which has been related to limited eddy propagation and feedback near the pole (Barnes and Hartmann 2010; Barnes et al. 2010).

Studies tend to agree on a generalized tendency of the NATL EDJ to move poleward (e.g. Lee et al. 2007) and experience dramatic shifts from N to S locations, describing a preferred transition loop of S–C–N–S EDJs (e.g. Franzke et al. 2011). Changes in eddy forcing can lead to latitudinal shifts of the EDJ (e.g. Lorenz and Hartmann 2003) although baroclinicity and the associated lower tropospheric heat fluxes also cause downstream influences on the EDJ (e.g. Novak et al. 2015). More specifically, meridional shifting has been linked to wave breaking, which acts to decelerate the zonal wind locally (e.g. Thorncroft et al. 1993; Benedict et al. 2004; Martius et al. 2007). Eddy momentum fluxes are poleward during Anticyclonic Wave Breaking (AWB) and equatorward during Cyclonic Wave Breaking (CWB), which accelerate the zonal flow north and south of the latitude of breaking, respectively (e.g. Rivière and Orlanski 2007; Strong and Magnusdottir 2008). As eddies supply momentum toward the EDJ core, they exhibit AWB (SW–NE tilting) signatures equatorward and CWB (NW–SE tilting) signatures poleward of the EDJ. That way, the location of the EDJ dictates different wave breaking types, which in turn help to maintain it in its shifted position, rendering distinctive wave breaking patterns for the three latitudinal regimes (Rivière 2009; Franzke et al. 2011; Novak et al. 2015).

On the other hand, recent studies indicate that the latitude alone does not fully account for the EDJ structure and its variability. Although latitudinal shifting represents the leading pattern of NATL EDJ variability (e.g. Athanasiadis et al. 2010), the NATL EDJ also experiences pulsing variations, which are more prominent in the presence of a strong subtropical jet (Eichelberger and Hartmann 2007) and when the EDJ approaches the pole (Barnes and Hartmann 2011). In addition, the EDJ can manifest zonal elongated patterns and changes in the tilt (e.g. Messori and Caballero 2015). Merged states of S EDJs with the subtropical jet have also been reported due to suppressed eddy activity by the strong zonal flow and a resulting shift in the balance of thermal and eddy-driving processes (Madonna et al. 2019). The EDJ latitude also provides incomplete information of the

large-scale circulation, since the dominant modes of variability represent a combination of at least changes in latitude, speed and width of the NATL EDJ (Monahan and Fyfe 2006). The three latitudinal regimes cannot fully account for the dominant weather regimes of the NATL such as European blocking, either, since the EDJ latitude struggles to identify complex flow configurations (Woollings et al. 2010; Madonna et al. 2017). Highly disturbed EDJs, such as strongly tilted and/or split EDJs, are particularly challenging because they represent regions of the EDJ space for which the latitude is poorly constrained and the predictability of the EDJ decreases (Frame et al. 2013).

Finally, future projections indicate a large spread of forced changes in the EDJ (e.g. Barnes and Polvani 2013; Zappa and Shepherd 2017). Although the multi-model mean response to increasing greenhouse gases concentrations involves weak poleward shifts and more peaked latitudinal distributions of the EDJ (Vallis et al. 2014; Iqbal et al. 2018), opposing effects of climate change can give rise to more complex patterns than simple shifts in EDJ latitude (Oudar et al. 2020; Lee et al. 2021), including an eastward elongation and narrowing of the EDJ (e.g. Peings et al. 2018), with potential impacts on regional climates. For these feasible scenarios, the associated impacts of future changes in the EDJ would be loosely captured by latitudinal descriptions of the EDJ, although its tilt, width and/or eastward extension were affected.

Consequently, the structure of the EDJ can be complex and challenging to describe using a single latitudinal index. Spatially-resolved zonal wind fields (Frame et al. 2011; Hannachi et al. 2012; Madonna et al. 2017; Dorrington and Strommen 2020) or sophisticated feature-based approaches (e.g. Koch et al. 2006; Strong and Davis 2008; Limbach et al. 2012; Peña-Ortiz et al. 2013; Spensberger et al. 2017) yield a more complete picture of the EDJ structure but they often lack an explicit measure of its attributes. Single metrics describing relevant aspects of the EDJ other than latitude, such as the tilt (Woollings and Balckburn 2012; Messori and Caballero 2015) or the waviness of the associated mid-latitude circulation (e.g. Cattiaux et al. 2016; Chen et al. 2016; Di Capua and Coumou 2016) have been proposed, albeit addressed in isolation. Ideally, a combination of parameters should be considered to ensure the representation of the EDJ structure. Acknowledging that the choice of such EDJ attributes depends on the purpose of the study, here we build a suite of EDJ parameters that allow a dissection of its structure beyond the well-established trimodality and, at the same time, a manageable treatment of complex EDJ configurations. Using these parameters, we aim to advance in the characterization of the wintertime NATL EDJ by addressing the following questions: Is there multimodality in EDJ parameters other than latitude and to what extent the latitudinal regimes discriminate other relevant aspects

of the EDJ? Are the proposed EDJ parameters enough to capture complex EDJ configurations, recurrent patterns and preferred transitions? Do we detect a measurable impact of these EDJ parameters on European surface climate conditions? Are we missing important information of regional climates if only EDJ latitude and intensity are considered?

This paper is structured as follows: Sect. 2 describes the datasets and methods. The EDJ parameters are defined in a separate Sect. 3, where we also illustrate some case studies. The main results are presented in Sect. 4, including the description of EDJ parameters (Sect. 4.1) and their relationships (Sect. 4.2). In Sects. 4.3 and 4.4, a multi-parametric approach is adopted to explore recurrent patterns of the EDJ and their transitions, respectively. The near-surface impacts associated with the EDJ parameters are discussed in Sect. 5. Finally, Sect. 6 summarizes the main conclusions.

## 2 Materials and methods

We use daily mean atmospheric data from the NCEP/NCAR reanalysis (Kalnay et al. 1996) at  $2.5^\circ \times 2.5^\circ$  spatial resolution for the winters (December–January–February, DJF) of the 1948–2020 period. Fields include daily mean temperature, and zonal and meridional wind components at different pressure levels. This dataset was preferred to other reanalysis products at high spatial resolution (e.g. ERA5; Hersbach et al. 2020) because it covers a longer period and spatial resolution is not critical for the diagnosis of the EDJ parameters (see details below). In addition, daily mean 2-m temperature and precipitation at  $0.25^\circ \times 0.25^\circ$  resolution was obtained from the E-OBS gridded dataset v23.1e (Haylock et al. 2008) for 1950–2020 in order to assess the European spatial patterns of near-surface responses to the EDJ parameters.

When required, monthly means are computed by averaging the daily values of each month. Daily and monthly anomalies are defined as departures of the fields from the climatological (full period) mean of the corresponding calendar day and month. On the other hand, several methods and diagnostics have been employed to assess the performance of the multi-parametric perspective of the NATL EDJ, as described next.

### 2.1 Clustering of EDJ parameters

To address the multi-faceted nature of the NATL EDJ and account for the diversity of recurrent patterns we have applied a k-means clustering to the daily winter series of EDJ parameters defined in Sect. 3, therefore partitioning the sample in a predefined number of clusters with different multi-parametric states of the EDJ (e.g. Wilks 2006). The k-means clustering assigns each day to one of the clusters

according to a metric distance (the sum of squared Euclidean differences with the clusters' centroids) so that the intra-cluster variance is minimized and the inter-cluster variance is maximized. To ensure equal weights on the Euclidean norm, the winter series of the EDJ parameters have been normalized and expressed as standardized anomalies. The algorithm is applied with 100 iterations to allow centroids to evolve enough from the random initial seeds. Results are reported for  $k=3$  and 4 clusters in order to assess if the multi-parametric approach is able to capture the three latitudinal regimes of the EDJ, and more complex 2D configurations of the EDJ (e.g. the four preferred spatial patterns of the zonal wind reported in Madonna et al. 2017). As some days are expected to be weakly tied to the assigned cluster, we repeated the analyses disregarding points with the largest distances (above the 90th percentile), without reporting noticeable differences.

### 2.2 Dynamical diagnostics

To explore in more detail the dynamics associated with variations in the EDJ parameters, we have computed several diagnostics, including the barotropic generation rate  $G$  and frequency of AWB and CWB. Following previous studies, the low-frequency (background,  $*$ ) and transient eddy ( $'$ ) components of daily mean temperature and horizontal wind are computed with a 10-day low-pass and a 2–6-day band-pass filter, respectively (e.g. Blackmon 1976; Woollings et al. 2010; Madonna et al. 2019). The transient eddy forcing of westerly momentum can be diagnosed with the horizontal E-vector (Hoskins et al. 1983):

$$\mathbf{E} = ((v'^2 - u'^2)/2, -u'v') \quad (1)$$

where  $u'$  and  $v'$  are the zonal and meridional filtered wind components at 300 hPa. E-vector indicates the propagation direction of transient eddies (opposite to the momentum flux) and its divergence corresponds to regions where transient eddies are accelerating the westerlies. Eddy-mean flow interactions are quantified with the barotropic generation rate  $G$  (Mak and Cai 1989), the scalar product of the horizontal E-vector and the deformation of the background flow  $\mathbf{D}$  due to stretching or shearing:

$$G = \mathbf{E} \cdot \mathbf{D}, \mathbf{D} = \left( \frac{\partial u^*}{\partial x} - \frac{\partial v^*}{\partial y}, \frac{\partial u^*}{\partial y} + \frac{\partial v^*}{\partial x} \right) \quad (2)$$

with  $u^*$  and  $v^*$  being the 300 hPa background winds. It characterizes the amount of kinetic energy extracted by the eddies from the background flow, so that when  $G$  is negative the eddies lose energy to the mean flow, thereby accelerating it.

Finally, to identify AWB and CWB we followed a modified version of the approach of Rivière (2009) and Michel

and Rivière (2011). The algorithm is based on the detection of local and instantaneous reversals of the PV gradient on isentropic surfaces. Circumglobal PV contours from 0 to 10 PVU are first delineated for each day with a step of 0.5 PVU. Segments oriented from east to west along the contour are then identified as wave breaking regions. To avoid sub-synoptic features, these reversals are required to extend over at least  $5^\circ$  in longitude. Similarly, reversals separated by less than  $5^\circ$  are considered as the same wave breaking. If latitude decreases (increases) along the points of the reversal, then the wave breaking is of AWB (CWB) type. This computation was restricted to the first point of the segment in the original method, but it is herein extended to the entire structure to account for large-scale Rossby wave breaking (e.g. Masato et al. 2012). For each day we obtain binary fields with the local occurrence of AWB and CWB, which are used to retrieve the frequencies of occurrence for selected periods. As AWB and CWB events do not occur at the same level (Martius et al. 2007), we average the frequencies over 300, 315, 330, and 350 K.

### 3 Definition of EDJ parameters

The daily parameters of the EDJ have been computed with a new methodology extending that employed in Woollings et al. (2010) for the characterization of the latitude and speed of the NATL EDJ. Zonal wind fields have been vertically averaged between 925 and 700 hPa and subsequently low-pass filtered to remove short-term fluctuations with periods lower than 10 days. To minimize local influences (e.g. orography, coastlines) in the diagnostics, all parameters are retrieved from zonal means of zonal wind over longitudinal sectors of  $60^\circ$  width, centered at each longitude of the spatial domain [ $90^\circ$  W– $30^\circ$  E,  $15$ – $75^\circ$  N]. These zonal means are denoted as  $U(\lambda, \varphi)$ , where  $\lambda$  is the half longitude of the sector and  $\varphi$  is the corresponding latitude. The parameters are derived from interpolants ( $0.5^\circ$  resolution) of the gridded fields employed in their computations using a cubic spline fit. The diagnosed parameters can be separated into two groups: basic parameters that are related to the wind speed and latitudinal position of the EDJ and additional parameters that describe the shape and configuration of the EDJ. An illustrative example of the method is provided in Fig. 1 to aid in the following explanations.

The basic parameters of the EDJ refer to the NATL [ $60^\circ$  W– $0^\circ$ ] sector only ( $U(\lambda_c, \varphi)$ , with  $\lambda_c = 30^\circ$  W) and are defined as follows:

- *Latitudinal position (Lat) and wind speed (Int)* (defined as in Woollings et al. 2010) *Lat* is the latitude  $\varphi_m$  of the maximum  $U(\lambda_c, \varphi)$  (brown horizontal line in the upper right inset plot in Fig. 1) and *Int* is simply the zonal wind at that latitude,  $U(\lambda_c, \varphi_m)$ . Note that *Lat* can only

account for a single wind peak, so it will select the strongest one in the presence of split or multiple jets.

- *Sharpness (Shar)* is defined as the difference between *Int* and the meridional mean of  $U(\lambda_c, \varphi)$  for all latitudes of the NATL (vertical line in the right inset plot of Fig. 1).

- *Poleward (Latn) and equatorward (Lats) flanks* are computed as the latitudes at each side of *Lat* where the  $U(\lambda_c, \varphi)$  values have decreased by half the sharpness (brown dashed lines in the right inset plot of Fig. 1). The search of *Latn* and *Lats* is restricted to the latitudes of the NATL sector, since they only exceptionally reach its boundaries.

The remaining parameters require the use of the sectoral means  $U(\lambda, \varphi)$  based on running averages of  $60^\circ$  longitude ( $\lambda \in [90^\circ$  W– $30^\circ$  E]), and are defined as follows:

- *Tilt (Til)* is defined as the slope of the linear regression comprising the tracked latitudes of *Lat* across the longitudinal sectors of the NATL (green line in Fig. 1). They are obtained by zonally tracking the wind maximum defined by *Lat* in the meridional profiles  $U(\lambda, \varphi)$  of the contiguous sectors, starting at  $\lambda_c$ , and proceeding to the east and west so that in each step the new latitude cannot change by more than  $\pm 2\Delta$ , where  $\Delta$  is the spatial resolution. The resulting latitudes  $\varphi_\lambda$  (yellow filled circles in Fig. 1) have associated wind speeds  $Int_\lambda = U(\lambda, \varphi_\lambda)$  (bottom inset plot in Fig. 1) and follow the zonal wind structure defined by *Lat*, regardless of the presence of other latitudinal maxima. The fitted latitudes are denoted as  $\varphi^*_\lambda$  and measure the tilt, which is expressed in  $^\circ$  N/ $60^\circ$  longitude.

- *Central longitude (Lon)* is defined as the average of the NATL longitudes, weighted by the square of their wind speed maxima  $Int_\lambda$  (vertical solid line in the bottom inset plot of Fig. 1), similar to the approach in Ceppi et al. (2014) for the diagnosis of the EDJ latitude. Note that this parameter does not necessarily coincide with the longitude of maximum  $Int_\lambda$ . Instead, its definition is intentionally restricted to the NATL sector, where *Lat* is detected, and informs on whether this latitudinal peak is zonally shifted with respect to  $\lambda_c$ .

- *Westward (Lonw) and eastward (Lone) extensions* are computed based on the absolute zonal gradient of  $Int_\lambda$ , similar to Peings et al. (2018) for the detection of the EDJ width. We start considering *Lon* and its adjacent longitude with higher  $Int_\lambda$ . This procedure is repeated, by incorporating in each step one longitude to the east or west of that interval, until [*Lonw*, *Lone*] contains half the contours of  $Int_\lambda$  over the NATL. If the western limit of the domain is reached before this condition is satisfied, the algorithm continues extending the eastern border, and vice versa (we obtain similar results if the loop ends at this stage). *Lone* and *Lonw* (dashed lines in the bottom inset plot of Fig. 1) render regions of high zonal gradients, if present, and inform on extensions/contractions of the EDJ and their zonal asymmetries.

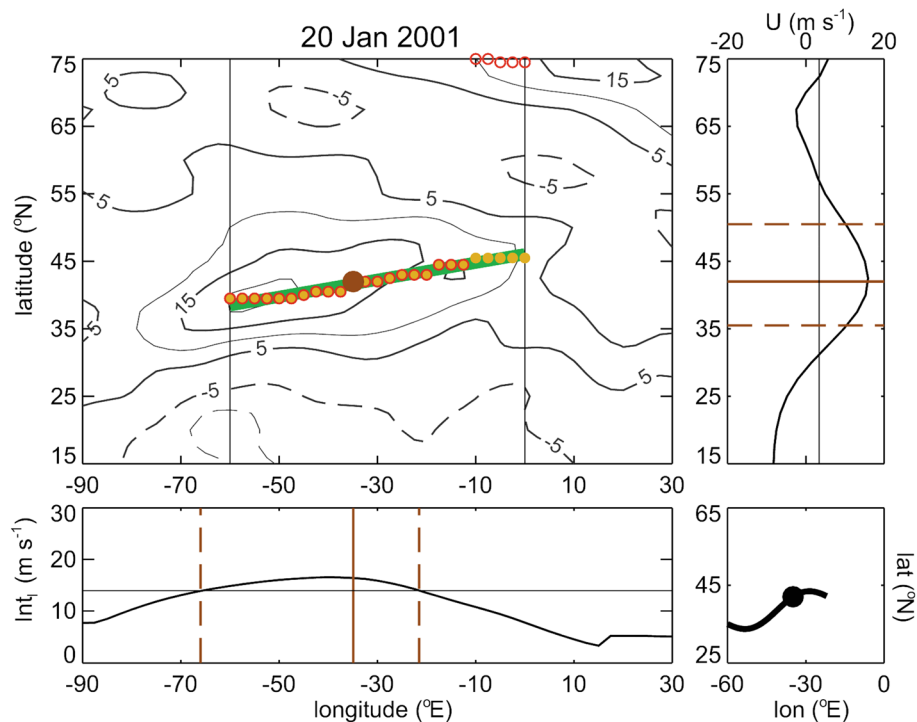


**Fig. 1** Example of the diagnosis of EDJ parameters for 20 January 2001. Main plot: 2-D low-pass filtered zonal wind at 925–700 hPa (contours in  $\text{m s}^{-1}$ ). Vertical lines identify the NATL sector ( $60^\circ \text{W}$ ,  $0^\circ$ ). The brown circle shows the location ( $Lat$  and  $Lon$ ) of the NATL EDJ. Circles filled in yellow denote the tracked latitudes of the NATL EDJ ( $\varphi_\lambda$  in the text) for running sectors of the NATL, and the slope of the fitted green line is the tilt ( $Til$ ). Open circles in red identify the latitude of maximum zonal wind ( $Lat_\lambda$  in the text) for the same sectors, whose spread measures the complexity of the EDJ ( $Dep$ ). Right inset plot: meridional profile of zonal wind for the NATL sector, with

the vertical line denoting the mean. The horizontal solid line identifies the latitude ( $Lat$ ) and dashed lines correspond to the northern and southern flanks ( $Lat_n$  and  $Lat_s$ ) of the EDJ. The wind value at  $Lat$  is the EDJ intensity ( $Int$ ), and the height of this peak defines the sharpness ( $Shar$ ). Bottom left inset plot: zonal wind at the tracked latitudes of the NATL EDJ ( $Int_\lambda$  in the text). The vertical line indicates the longitude ( $Lon$ ) and dashed lines identify the western and eastern boundaries ( $Lon_w$  and  $Lon_e$ ) of the EDJ. Bottom right inset: snake-like plot of the EDJ parameters (see main text for details)

- *Departure* ( $Dep$ ) measures the spread of latitudinal wind maxima across the NATL (i.e. how well the EDJ can be described by a single continuous structure). To do so, the latitudinal position of the EDJ,  $Lat$ , inferred from  $U(\lambda_c, \varphi)$  has been computed for the other sectors spanning the longitudes of the NATL, and denoted as  $Lat_\lambda$ . For single well-defined EDJs,  $Lat_\lambda$  (open red circles in Fig. 1) will coincide with  $\varphi_\lambda$  (the tracked latitudes of the  $Lat$  peak, yellow filled circles in Fig. 1), as in the example of Fig. 1.  $Dep$  is then computed as the root mean squared difference (RMSD) of  $Lat_\lambda$  with respect to  $\varphi_\lambda^*$ , which minimizes any influence of the tilt in the definition. Note that complex structures such as double EDJs will have large  $Dep$  values, but the latter does not involve large tilts, and vice versa. This parameter is somewhat similar to, but should not be confounded with, other diagnostics describing the waviness of the mid-latitude flow: a wavy pattern can occur for single EDJs with low  $Dep$  values (e.g. Greenland block and S EDJs; Woollings et al. 2010; Davini et al. 2012).

The EDJ parameters can be represented collectively by means of snake-like plots such as that shown in the bottom right inset of Fig. 1. These plots consist of a dot and a line. The former identifies the EDJ position ( $Lon$  and  $Lat$ ), with the size proportional to the EDJ intensity ( $Int$ ). The length and thickness of the line informs on the zonal extension (from the western,  $Lon_w$ , to the eastern,  $Lon_e$ , boundary) and latitudinal width (defined as the difference between the northern and southern latitudinal edges, i.e.  $Lat_n$  minus  $Lat_s$ ) of the EDJ, respectively. The orientation and waviness of the line is proportional to the EDJ tilt ( $Til$ ) and the spread of latitudinal maxima across the NATL ( $Dep$ ), respectively.

Finally, the above metrics of the EDJ are complemented with a 2D daily representation of the EDJ width. It is based on an extension of the  $Lat_n$  and  $Lat_s$  definition to all sectors of the considered domain, therefore yielding the latitudinal edges,  $Lat_{n,\lambda}$  and  $Lat_{s,\lambda}$ , for the zonally-varying wind peaks  $Lat_\lambda$ . These parameters provide a more explicit description of the EDJ, and account for spatial variations in its structure,

which can be sensitive to the chosen region (e.g. Ordoñez et al. 2019). As in feature-based algorithms, this method delivers daily gridded binary (0/1) fields of the EDJ over the considered domain, with 1 identifying the latitudes of the EDJ core at each longitude. These daily snapshots will be employed to compute maps with the frequencies of occurrence of the EDJ over specific periods. That way, for a given period, the method provides frequency maps of the EDJ and the time evolution of single parameters. An illustrative example is shown in the supplementary material for 28 December 2010–10 January 2011, which corresponded to one of the largest negative NAO events on record (Figure S1).

For most of these parameters, other alternative definitions were tested, picking those that best performed (by subjective inspection of selected cases) and were robust to methodological choices (selection of the vertical level, spatial domain, filtering of the daily fields, etc.). We verified that the results are not substantially affected by other definitions of the EDJ latitude (e.g. Ceppi et al. 2014), when a single (850 hPa) vertical level is used instead of the vertical average, or if some methodological steps (e.g. low-pass filter of daily fields, spline interpolation) are omitted. The method was further tested by applying a land mask to reduce the influence of orography (e.g. Messori and Caballero 2015). This approach also yielded similar results, except for the *Lone* and *Lonw* extensions, which become ill-defined (and make no sense) if zonal winds over land are ignored. On the other hand, the main conclusions of this manuscript remain if the analysis is restricted to the satellite period of the reanalysis (1979–2020). Finally, the retrieved series of winter EDJ parameters are in good agreement with those obtained from ERA5 fields at  $0.5^\circ \times 0.5^\circ$  spatial resolution (correlation coefficients typically above 0.9,  $p < 0.01$  and RMSD substantially lower than the standard deviation), suggesting that the method is robust to the reanalysis product and spatial resolution.

Overall, the proposed parameters provide robust estimates of major features of the EDJ that have been considered relevant in the literature. In addition, they rely on relatively simple metrics rather than very detailed diagnostics, which would require more complex and sophisticated developments. The EDJ parameters can be used in combination or isolation, attending to the specific features of the EDJ one is interested in, and hence offer multiple applications, some of which are illustrated in the following sections.

## 4 Results

### 4.1 Description of EDJ parameters

First, we describe the daily winter distributions of the EDJ parameters (Fig. 2). Both the intensity (*Int*, red line

in Fig. 2a) and sharpness (*Shar*, blue) show near-Gaussian distributions, in agreement with previous studies on the wind speed of the EDJ (e.g. Woollings et al. 2010; Dorrington and Strommen 2020). These distributions are shifted by less than  $5 \text{ m s}^{-1}$ , which is approximately the climatological winter mean of the NATL zonal wind over  $[15, 75^\circ \text{ N}]$ . Interestingly, the mean value of both parameters is slightly underpopulated as compared to a perfect Gaussian distribution, and visually suggests some tendency for a double peaked distribution. The distribution of the EDJ latitude (*Lat*, red line in Fig. 2b) captures the trimodality of the EDJ, with preferred positions in southern, central and northern latitudes of the NATL. These peaks are not present in the poleward (*Latn*, yellow) and equatorial (*Lats*, blue) flanks of the EDJ, arguably due to the influence of the wind speed, which is used in the definition of these parameters and can obscure the trimodality of the EDJ (Strommen 2020). *Latn* shows a distribution skewed toward low values, but with a pronounced peak in the north ( $\sim 60^\circ \text{ N}$ ), and a modest one in central latitudes ( $\sim 50^\circ \text{ N}$ ), matching the poleward boundaries of N and C EDJs, respectively. However, the northern peak of *Latn* is more populated than that of *Lat*, and the opposite is observed for the central peak, indicating that C EDJs can extend their poleward flanks to high latitudes. There is not a discernible southern peak in *Latn*, and hence S EDJs set their poleward boundaries over a wide range of mid-latitude locations, including those typical of C EDJs. Differently, the distribution of *Lats* is skewed towards high values, with no obvious peaks. There is a broad maximum from  $\sim 30\text{--}45^\circ \text{ N}$ , embedding the equatorward flanks of S and C EDJs, whereas the southern boundary of N EDJs becomes diluted in the mid-latitudes. The sharp decrease of *Lats* towards subtropical latitudes is more pronounced than that in *Lat* and suggests a well-constrained equatorward flank of S EDJs, likely caused by the presence of deep subtropical easterlies. A similar behavior is found at high latitudes for the poleward flank of N EDJs. Therefore, N and S EDJs have their outermost flanks constrained, whereas C EDJs enjoy comparatively larger latitudinal widths (as measured by the difference between *Latn* and *Lats*; not shown).

The longitude of EDJ (*Lon*, red line in Fig. 2c) is also Gaussian distributed and the frequency peak occurs in the central NATL. In at least two thirds of the days, the western (*Lonw*, yellow) and eastern (*Lone*, blue) extensions of the EDJ are also detected within the NATL, and their frequencies of occurrence decrease rapidly towards continental areas. *Lonw* and *Lone* tend to peak near the tails of the *Lon* distribution. The eastern peak of *Lonw* corresponds to easternmost EDJs extending their wind maxima towards Europe, while the western peak of *Lone* denotes EDJs that are confined to the western half of the NATL. This is supported by composites of zonal wind and EDJ parameters for the upper and lower terciles of *Lon* (Fig. 3a).

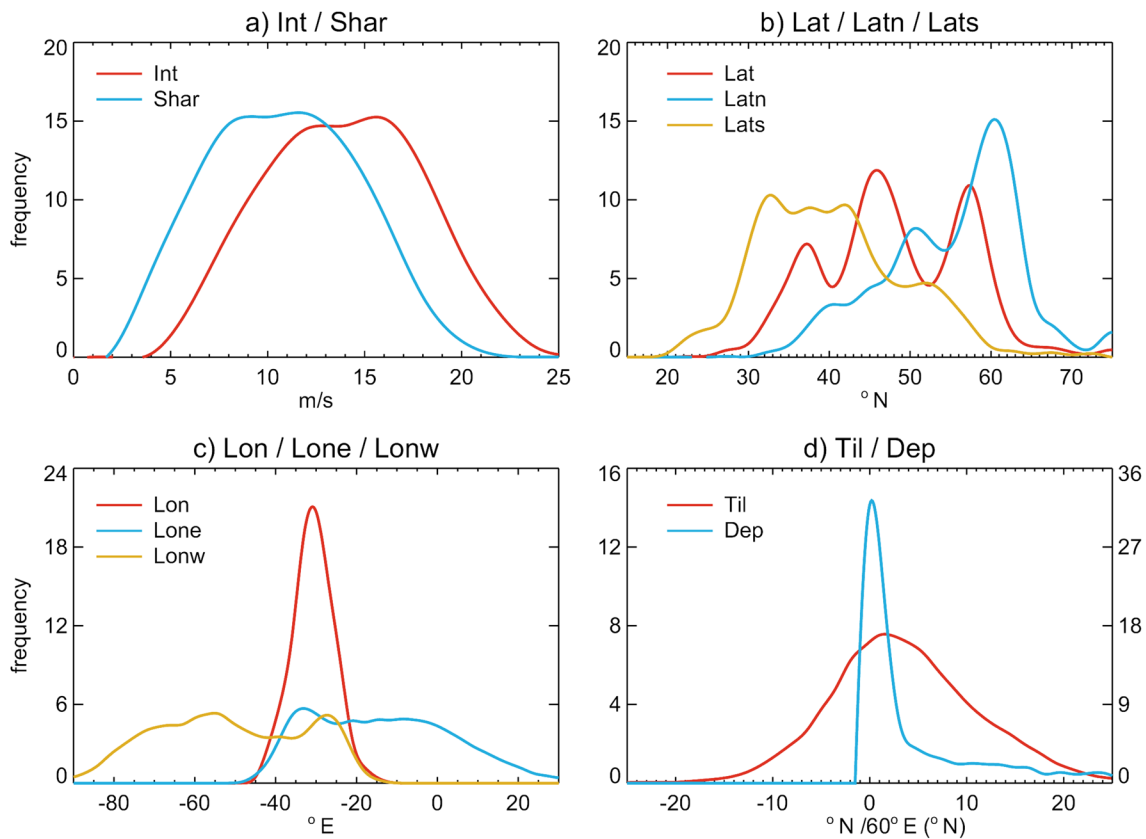


**Fig. 2** Climatological mean frequency distributions of the winter EDJ parameters for the 1948–2020 period: **a** intensity and sharpness; **b** latitude and poleward and equatorward edges; **c** longitude and eastward and westward extensions; **d** tilt and departure. For each plot, the

PDFs are computed using bins of  $2 \text{ m s}^{-1}$ ,  $2.5^\circ \text{ N}$ ,  $3^\circ \text{ E}$  and  $1.5^\circ \text{ N}$ , and fitted with a polynomial spline. The frequency of the *Dep* parameter is shown with respect to the right y-axis scale in **d**

The tilt of the EDJ (*Til*, red line in Fig. 2d) also displays a near-Gaussian distribution, with frequency maxima at small values (i.e. zonal EDJs) and a clear skewness towards positive tilts (i.e. SW–NE inclinations). Positive values range up to  $25^\circ \text{ N}/60^\circ$  longitude, which is close to the difference between the northern and southern peaks of *Lat*. There is a relatively high frequency of negative tilts (NW–SE). These configurations tend to occur during N and S EDJs with zonal extensions towards western and eastern regions, respectively (Fig. 3b). On the other hand, high positive tilts are typical of C EDJs, but with a non-negligible contribution of N EDJs. Thus, the latitudinal position of the EDJ does not fully determine its orientation.

The departure parameter (*Dep*, blue line in Fig. 2d) measures the degree of complexity of the EDJ (i.e. fluctuations in latitudinal position along the NATL) and shows a highly peaked distribution, with about half of the days displaying very low values ( $< 2^\circ$ ). This distribution is a desirable aspect, and confirms that for many (but not all) cases the EDJ shows a well-defined continuous structure across the NATL. Days in the low *Dep* tercile feature strong zonal EDJs, characterized by prominent zonal winds over the central NATL and a

weakening towards the southeast (blue contours in Fig. 3c). Differently, the composite of EDJ occurrence for days with large deviation of latitudinal peaks shows hints of a split pattern, with branches in the northeastern and southwestern NATL (shading in Fig. 3c). Although C EDJs are much less common during high *Dep* values, the opposite is not true, and there is not a clear correspondence between *Dep* and the latitudinal EDJ regimes.

In summary, the selected parameters describe the location, zonal extension and shape of the EDJ. As stated in the Introduction, shifting and pulsing variations of the EDJ have been linked to changes in eddy forcing and wave breaking, which act to amplify and maintain the EDJ in its disturbed state (e.g. Eichelberger and Hartmann 2007; Rivière and Orlanski 2007; Barnes and Hartmann 2011). Here, we briefly explore if this also applies to other manifestations of the EDJ variability. Figure 4 summarizes the dynamical field signatures associated with selected EDJ parameters, as measured by daily-based correlations with the barotropic generation rate *G* (shading) and the 10-day running frequency of AWB and CWB (contours in purple and pink, respectively). Given the large sample, significance is not

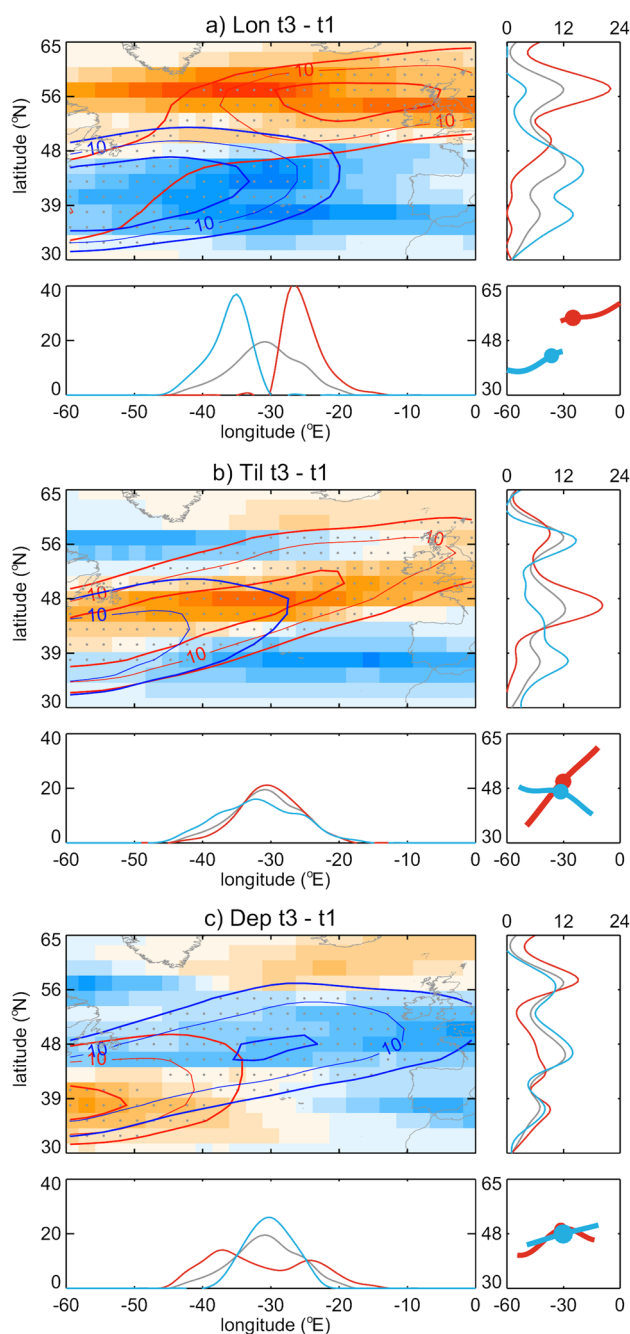


**Fig. 3** Difference of EDJ frequency (shading; in percentage of days) for winter days with high (upper tercile) minus low (lower tercile) values in the NATL EDJ: **a** longitude; **b** tilt; **c** departure. The frequency is computed in percentage with respect to the total number of days of each category. Red and blue shading show positive and negative frequency anomalies with contour interval of 10%. Red and blue lines show the composited zonal wind at 925–700 hPa ( $\text{m s}^{-1}$ ) for the upper and lower tercile, respectively. Grey dots indicate significant differences at  $p < 0.01$ . The bottom and top right insets show the frequency distribution of the EDJ longitude and latitude, respectively, for the climatology (grey) and the upper (red) and lower (blue) tercile categories. The PDFs are shown in percentage with respect to the total number of days in each category. The bottom right inset shows the composited EDJ parameters for the upper (red) and lower (blue) tercile category

substantially altered when autocorrelation is considered. The patterns are also consistent with dynamical composites for the upper and lower terciles of the EDJ parameters (not shown).

Overall, daily variations of EDJ parameters are associated with distinctive dynamical patterns. When the EDJ strengths (Fig. 4a), eddies extract kinetic energy upstream and accelerate the mean flow downstream, resulting in a zonally-oriented dipole in  $G$ . This is consistent with reduced CWB activity on the western NATL, where eddies grow at expense of the zonal flow, and the supply of poleward momentum fluxes by AWB on the equatorward flank of the downstream EDJ. The limited variety of wave breaking types agrees with the reported effect of strong EDJs on eddies, which tend to be reflected on the poleward flank of the EDJ and break anticyclonically on its equatorward side (Woollings et al. 2018, and references therein). Differently, latitudinal variations of the EDJ feature a consistent pattern of eddy-mean flow interactions across the NATL (Fig. 4b), although this may reflect mixed influences of EDJ transitions from different latitudinal regimes. High frequency of AWB over central and eastern Atlantic steers the EDJ northwards, which is consistent with the dominance of this type of wave breaking during poleward migrations of the EDJ (e.g., Franzke et al. 2011). In turn, northward-shifted EDJs limit the occurrence of CWB on its poleward side by the constraining effect of latitude on the propagation and breaking of eddies (e.g., Barnes et al. 2010). Conversely, a southward deflection of the EDJ implies enhanced CWB frequencies on its poleward flank, as observed during S regimes and negative NAO phases (e.g., Benedict et al. 2004; Franzke et al. 2011). The dynamical patterns associated with changes in the latitudinal flanks of the EDJ are similar to those of  $Lat$ , but display small meridional shifts towards the corresponding edge (not shown).

Variations in other EDJ parameters are substantially influenced by AWB. The comparatively weaker role of CWB in terms of magnitude and/or spatial extent could be related to its lower climatological frequency (e.g., Martius et al. 2007) and eddy momentum fluxes (Rivière 2009). Changes in the EDJ structure are sensitive to the specific location of AWB, so that the same anomaly in AWB may have different effects depending on its region of occurrence. The pattern of wave breaking associated with longitudinal variations (Fig. 4c) somewhat resembles that found for  $Lat$ , supporting that poleward EDJs also tend to extend farther downstream (Fig. 3a). However, there are also differences, as evidenced in the eddy forcing, which displays a zonal tri-pole. Eastward shifts of the EDJ (Fig. 4c) reflect high AWB frequency over the eastern NATL and large eddy forcing at the end of the storm track. During westward shifts of the EDJ, the suppression of eddy feedbacks at the EDJ's exit by the lack of AWB impedes the maintenance of local

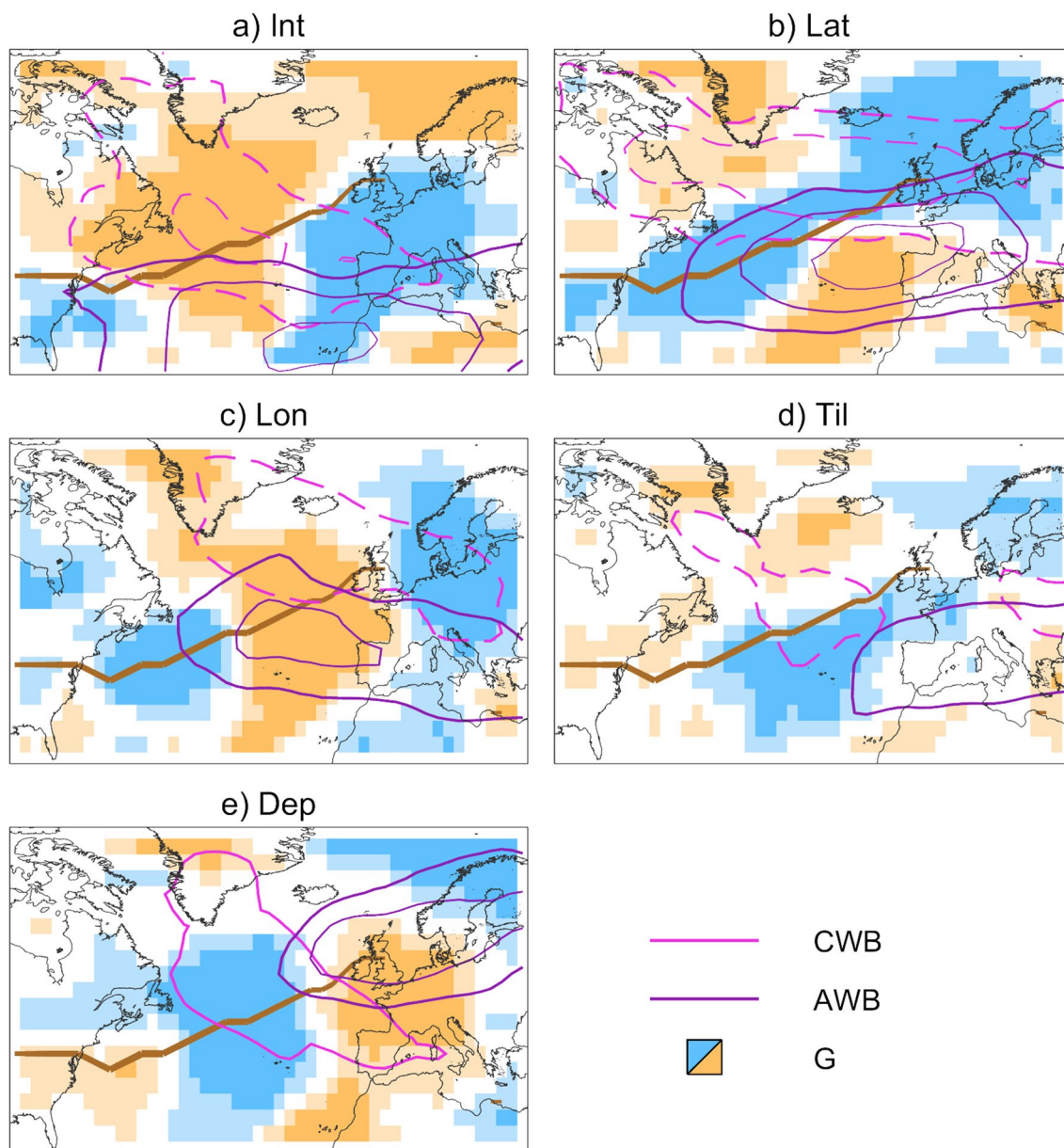


**Fig. 4** Pearson's correlation coefficient between daily wintertime series of dynamical diagnostics and the following EDJ parameters: **a** intensity; **b** latitude; **c** longitude; **d** tilt; **e** departure. Dynamical fields include the barotropic generation rate at 300 hPa (G, shading) and 10-day wave breaking frequency (contours, with AWB in purple and CWB in pink). Red and blue shading denotes positive and negative correlations, with light/dark colors indicating significance

at  $p < 0.1/0.001$ . Solid and dash contours represent significant correlations at  $p < 0.1$  with contour interval of 0.1. For a given type of wave breaking, we only show the signed correlations with the highest absolute coefficient, omitting opposite correlations to improve readability. Brown lines follow the climatological zonal wind maxima at 925–700 hPa, with the thickness proportional to their magnitude (only zonal winds stronger than  $7 \text{ m s}^{-1}$  are shown)

westerlies, and CWB further contributes to reinforce the EDJ upstream. On the other hand, European AWB modulates the zonal asymmetries of the EDJ, with the latitude of AWB occurrence determining the specific EDJ parameter that is being affected. AWB over southern Europe is related to increased tilt (Fig. 4d), whereas disturbed EDJs (Fig. 4e) involve AWB at comparatively higher latitudes. These two patterns of AWB and the associated EDJ structure resemble

those obtained for the Atlantic ridge and blocking weather regimes, respectively (Michel and Rivière 2011; Sousa et al. 2021). We do not identify a similar relationship between the latitude of CWB and variations in the zonal asymmetries of the EDJ. Although CWB tends to act against positive tilts (Fig. 4d) by confining the EDJ to southern latitudes, it can also favor disturbed configurations when accompanied by downstream AWB at high latitudes (Fig. 4e).

## 4.2 Relationships between the EDJ parameters

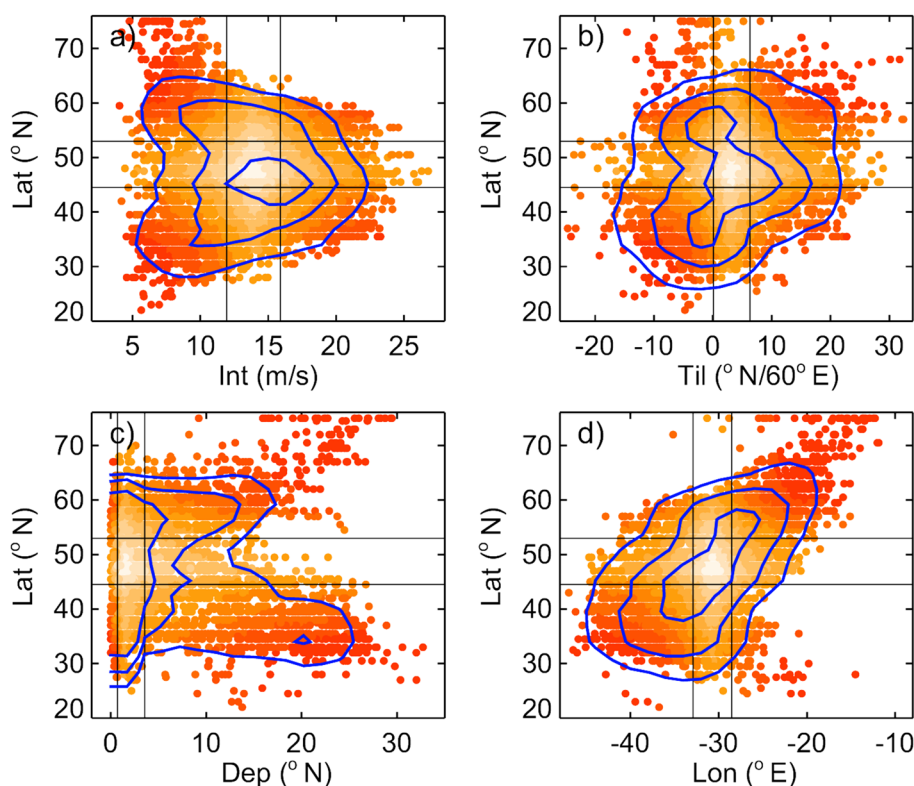
We next describe the most important relationships between the different parameters of the EDJ on a seasonal and daily basis. Several parameters exhibit statistically significant correlations of their winter mean values on interannual and longer time scales. EDJs located at lower latitudes tend to display westward-shifted positions ( $r(Lat, Lon) = 0.64$ ,  $p < 0.01$ ). The relationship also applies to the longitudinal boundaries of the EDJ ( $Lone$  and  $Lonw$ ), and may simply reflect the land-sea distribution of the NATL, including the reported influences of Greenland's orography (White et al. 2019) and the life cycle of baroclinic eddies (e.g. Novak et al. 2015) on the downstream development of EDJ regimes. The EDJ latitude also correlates with the tilt ( $r(Lat, Til) = 0.40$ ,  $p < 0.05$ ) on a seasonal basis. This result is consistent with previous studies that have also reported an increase in EDJ tilt as it shifts north (e.g. Woollings et al. 2010; Novak et al. 2015). The characteristic SW-NE tilt seems to be unique of the NATL EDJ and has been related to an unconstrained variability due to the presence of a weak subtropical jet (Barnes and Hartmann 2011) and dominance of AWB in the NATL (Martius et al. 2007; Rivière 2009). The correlation is not very high, though, likely due to the additional, albeit weak, influence of CWB on the EDJ tilt (Fig. 4d). There is also a negative correlation between EDJ intensity and complexity ( $r(Int, Dep) = -0.66$ ;  $p < 0.01$ ), indicating that weaker EDJs tend to display a larger spread in their latitudinal locations.

These asymmetries are smoothed in the NATL zonal average, leading to blurred and weak latitudinal peaks. If the tilt causes comparable effects on intensity, they are weak since we do not identify significant correlations between these parameters.

On the other hand, seasonal mean conditions can also modulate the daily variability of the EDJ. In particular, strong EDJs have been associated with a reduced latitudinal variability (Woollings et al. 2018), as captured by the correlation between the mean  $Int$  and the standard deviation of daily  $Lat$  in each winter ( $r = -0.52$ ;  $p < 0.05$ ). The reduced capability of strong EDJs to experience latitudinal shifting has been related to enhanced refraction of wave breaking on the poleward flank of the EDJ, which limits the degree of meridional asymmetry in wave breaking activity required for latitudinal shifts (Woollings et al. 2018). We find that this link is also extensible to other parameters of the EDJ such as  $Lon$ ,  $Til$  and  $Dep$  whose variance decreases when the EDJ becomes stronger (in all cases with negative correlations of at least  $-0.47$ ;  $p < 0.05$ ). Similarly, an enhanced winter mean  $Dep$  increases the variability of most EDJ parameters ( $Lat$ ,  $Lon$ ,  $Til$ ,  $r > 0.49$ ;  $p < 0.05$ ), a result somewhat expected for complex and/or ill-defined EDJ patterns.

The mentioned relationships of the winter mean parameters should not be extrapolated to daily time scales. Associations between the EDJ parameters on daily scale have been explored with 2D scatter plots and frequency distributions for each pair of parameters (see Fig. 5 for selected pairs

**Fig. 5** Winter scatter plots of the EDJ latitude ( $^{\circ}N$ ) with respect to other parameters of the NATL EDJ: **a** intensity ( $m s^{-1}$ ); **b** tilt ( $^{\circ}N$ ); **c** departure ( $^{\circ}N$ ); **d** longitude ( $^{\circ}E$ ). Blue contours show the median and the 75th and 90th percentiles of the 2-D frequency distribution. The vertical and horizontal lines denote the lower and upper terciles of the EDJ parameters. The color of the dot is degraded (from white to red) according to its degree of extremeness



including *Lat*). To better illustrate the structure of the EDJ during specific combinations of parameters, we also show composites of the 2D EDJ for predefined regions of the 2D parameter space with unexpectedly high density (Fig. 6). To identify these regions, we simply counted the number of days for each combination of terciles of the two parameters (a total of nine quadrants in the 2D parameter space). Then, we picked the tercile-based combinations that display frequencies above the expected probability of occurrence for independent samples of the same size (~ 11%). While this approach does not necessarily capture the peaks of the 2D frequency distribution, it provides a first approximation to the most preferred combinations of parameters. We also note that the tercile groups of *Lat* do not perfectly match with the three latitudinal regimes. In particular, the first tercile

group includes S EDJs and EDJs located in the southernmost latitudes of the central peak. However, for simplicity, we will keep the terminology of N, C and S EDJs for the tercile groups of *Lat*.

The results confirm some of the correlations found on seasonal scales (e.g., an eastward shift of the EDJ as it moves to higher latitudes; Fig. 5d). However, other relationships reported for the winter mean parameters become more complex (e.g., the relationship of *Lat* and *Til*; Fig. 5b) or deviate from the linearity at daily scales (e.g. *Lat* and *Int*; Fig. 5a). The *Lat* vs *Int* space (Fig. 5a) displays a ‘U-shaped’ distribution, like that reported between EDJ latitude and NAO (Strommen 2020). Accordingly, C EDJs tend to be stronger than EDJs located near the N and S peaks. Indeed, the most populated terciles of the

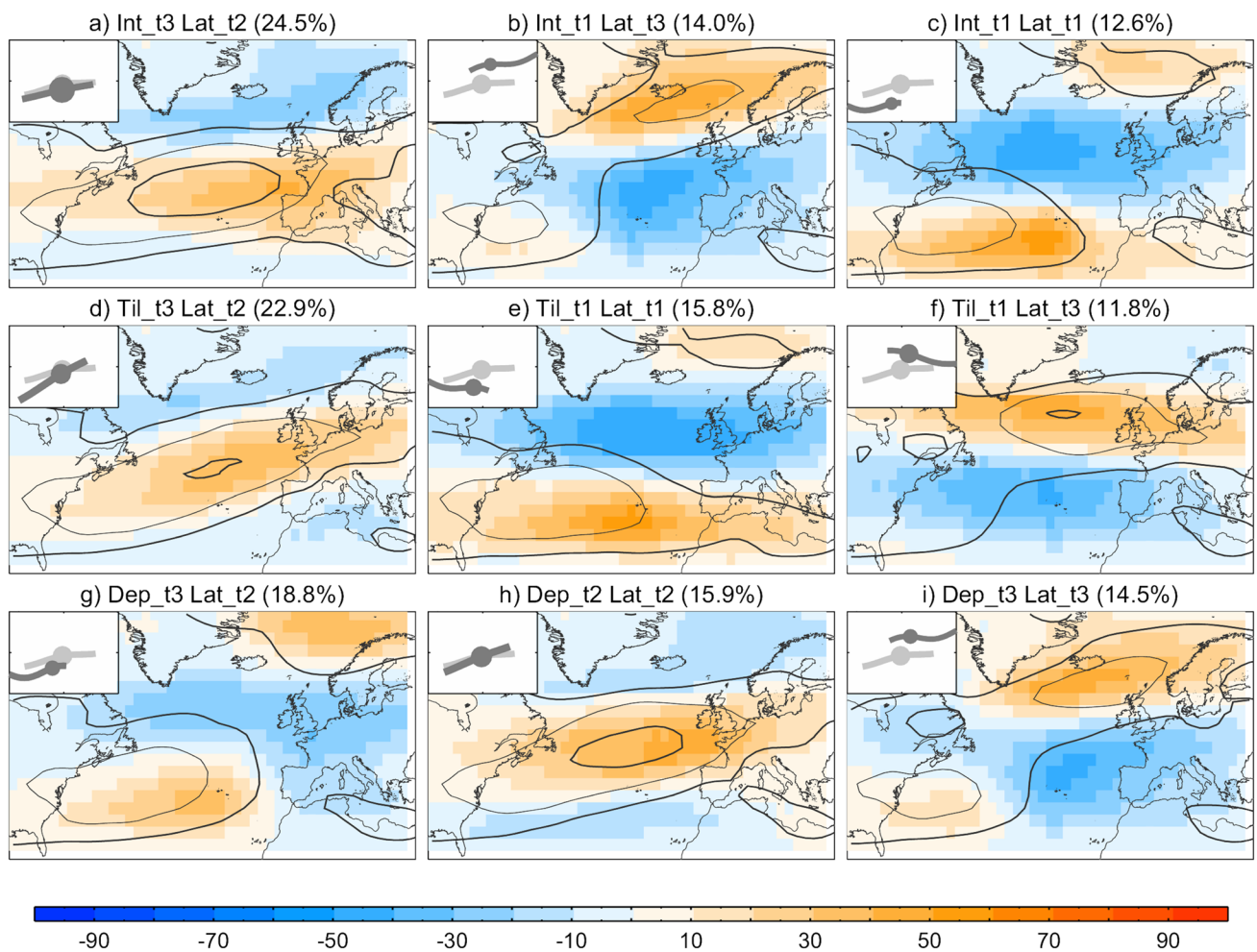


**Fig. 6** Composites of zonal wind at 925–700 hPa (contours, in  $\text{m s}^{-1}$ , contour interval of  $5 \text{ m s}^{-1}$  starting at  $5 \text{ m s}^{-1}$ ) and EDJ frequency anomalies (shading, in percentage of days) for the preferred combinations of EDJ parameters’ pairs: **a–c** latitude and intensity; **d–f** latitude and tilt; **g–i** latitude and departure. The top left inset of each panel shows snake-plots of the mean EDJ configuration for the composite (dark grey) and the climatology (light grey). The selection is based on

the relative frequency of days in each ninth of the 2-D space (Fig. 4), as defined by the tercile categories (t1—lower tercile; t2—middle tercile; t3—upper tercile) of the EDJ parameters. For the same pair of EDJ parameters (row panels), the most populated ninths are sorted by frequency (from left to right, in decreasing order) and identified in the title of the panels

2D *Lat-Int* parameter space correspond to strengthened C EDJs and weakened N and S EDJs (Fig. 6a–c), likely explaining the tendency for a double peaked *Int* distribution (Fig. 2a). Figure 5a also evidences the decrease in latitude variability during strong EDJs, which is also observed for other EDJ parameters (e.g. *Lon* and *Til*; not shown). Therefore, weak EDJs can manifest a wider range of tilts than strong EDJs and occur more frequently in shifted locations (longitudes and latitudes) of the NATL.

The *Lat-Til* space (Fig. 5b) shows that equatorward-shifted EDJs tend to be more biased towards negative tilts (i.e., NW–SE orientation) than EDJs at higher latitudes, in agreement with the correlation found at seasonal scales. However, a closer inspection reveals that this relationship is not fully linear, and negative tilts are comparatively more common for N EDJs than for C EDJs (see also the composite of Fig. 3b). Accordingly, preferred combinations correspond to SW–NE oriented C EDJs and NW–SE oriented S and N EDJs (Fig. 6d–f). The last combination shows comparatively lower frequencies, in agreement with the large diversity of N EDJ tilts and the non-systematic increase of poleward locations as the tilt increases (Fig. 3b). These non-linear aspects may also explain some apparent discrepancies found in the literature. For instance, while N EDJs can display the largest tilts (Fig. 5b), and are, on average, more tilted than other latitudinal regimes (Woollings et al. 2010), tilted patterns are often found as a variation of C EDJs (Madonna et al. 2017; Dorrington and Strommen 2020).

Finally, a strong non-linear behavior is found between *Dep* and several parameters, including *Lat* (Fig. 5c) and *Lon*. Due to the highly peaked *Dep* distribution, its terciles are biased to low values, therefore defining groups with extremely low ( $< 1^\circ$  N), low ( $\sim 1\text{--}3^\circ$  N) and all other (moderate-to-high) *Dep* values. With this stratification, recurrent combinations include C EDJs with low *Dep* and N EDJs with moderate-to-high *Dep* (Fig. 6h, i). Perhaps surprisingly, the most likely one corresponds to C EDJs with large departures in latitudinal position (moderate-to-high *Dep*). Despite being embedded in the C regime, these EDJs are shifted to southern latitudes and the western NATL (Fig. 6g). Thus, zonal variations in latitudinal position can increase rapidly as EDJs move apart from the undisturbed central peak. In fact, the highest values of *Dep* occur for N and S EDJs (Fig. 5c), likely denoting split flow configurations with poleward and equatorward branches of the EDJ, for which *Lat* can only capture one of them. The increase of *Dep* with latitudinal shifting seems to be larger towards the subtropics, suggesting that split patterns tend to be detected as S EDJs. Indeed, the fourth preferred combination of *Lat-Dep* terciles (S EDJs with moderate-to-high *Dep*) resembles the southward shifted pattern of Fig. 6g, but with a more pronounced split configuration (not shown).

### 4.3 Recurrent configurations of the EDJ

We have shown that the same latitudinal regime can exhibit a diversity of patterns, depending on the specific aspect of the EDJ that is being scrutinized. This reveals a multiplicity of structures beyond the traditional three latitudinal regimes that can be addressed with an integrated multi-parametric assessment of the EDJ. To dissect the multi-faceted nature of the NATL EDJ and account for the diversity of recurrent patterns we have applied a k-means clustering to the daily EDJ parameters (as described in Sect. 2).

We start showing the results when only three clusters ( $k=3$ ) are defined. As expected, they largely capture the three preferred latitudinal positions of the EDJ, which is the most distinguishable aspect of the EDJ, and are therefore referred to as C3, N3 and S3 clusters (Fig. 7a–c). This is supported by histograms of *Lat* for the days assigned to each cluster (green lines in the right panels of Fig. 7). The agreement with the three latitudinal regimes, i.e. the clusters obtained using only *Lat* (Figures S2a–c of the Supplementary Material), is not perfect though. On average, almost two thirds of the days in the three latitudinal regimes are classified in their multi-parametric counterparts. The remaining days often correspond to EDJs with parameters that are more characteristic of other clusters' centroids (Figure S3). For example, C EDJs absent in the C3 cluster are often associated with relatively weak and westward shifted EDJs, which are characteristic signatures of the S3 cluster. Thus, a measurable influence of the other EDJ parameters exists, which is expected to be more important as EDJs move apart from the main peaks that define the centroid latitudes. Therefore, the multi-parametric space assists in the identification of EDJ structures, emphasizing distinctive signatures of the EDJ other than latitude. From this multi-faceted perspective, C3 EDJs are stronger than N3 and S3 EDJs, which in turn display different longitudinal position (eastern and western NATL, respectively), tilt (smaller for S3 EDJs) and degree of zonal departures (higher for S3 EDJs) (Fig. 7a–c).

The multi-parametric approach can thus inform on the 2D structure of the EDJ. Indeed, the spatial patterns of N3 and C3 EDJs resemble two of the three clusters of the 2D zonal wind presented in Madonna et al. (2017). The third pattern found therein corresponded to strongly tilted or split EDJs comprising a comparable frequency of N and S EDJs (the so-called mixed pattern). While our S3 cluster also shows reminiscent signatures of a split flow, it does not show a balanced frequency of N and S EDJs, being clearly dominated by EDJs at southern latitudes (southern flank of the central peak and S EDJs). The composites of Fig. 7a–c and the associated distributions of EDJ parameters (not shown) suggest that tilted and split-like configurations typical of the mixed pattern are relatively common in the N3 and S3 cluster, respectively.

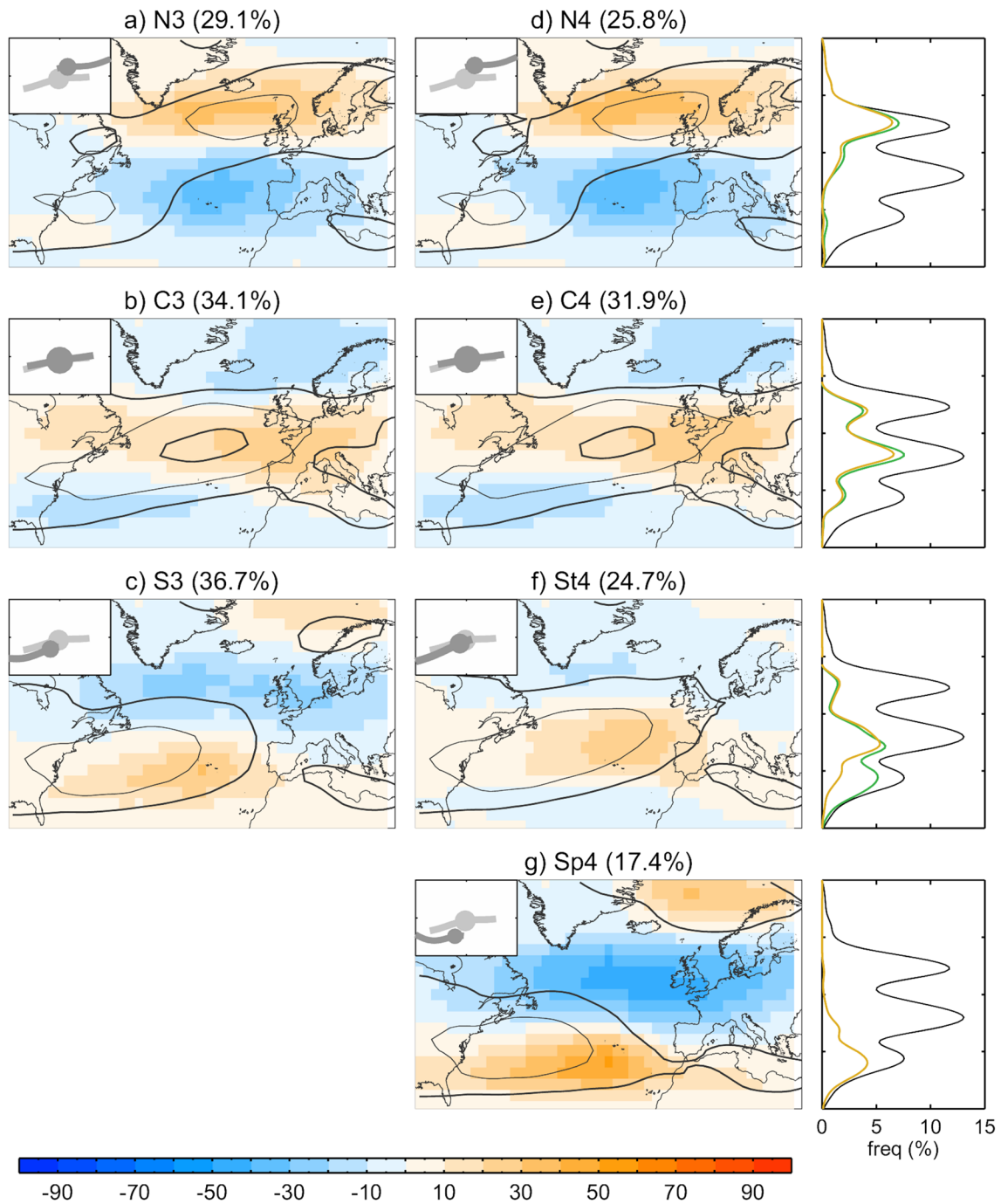


**Fig. 7** Composites of zonal wind at 925–700 hPa (contours, in  $\text{m s}^{-1}$ , contour interval of  $5 \text{ m s}^{-1}$  starting at  $5 \text{ m s}^{-1}$ ) and EDJ frequency anomalies (shading, in percentage of days) for days assigned to each cluster of the NATL EDJ parameters. Results are shown for: **a–c** three clusters (N3, C3 and S3); **d–g** four clusters (N4, C4, St4 and Sp4). The relative frequency of winter days in each cluster is shown in the

title. The top left inset of each panel shows snake-plots of the mean EDJ configuration for each cluster (dark grey) and the climatology (light grey). Right plots show the frequency distribution of NATL EDJ latitude for the  $k=3$  (green) and  $k=4$  (yellow) clusters displayed in the same row (in percentage with respect to the total number of winter days). Black line is the climatology

A less satisfactory result is the inability of the three multi-parametric clusters to better isolate the southern peak of the latitudinal distribution, which was also challenging in previous studies using high-dimensional clustering (Hannachi

et al. 2012; Madonna et al. 2017; Dorrington and Strommen 2020). Consequently, we extend the analysis of multi-parametric states of the EDJ to  $k=4$  clusters. In this case, one gets EDJs at three distinguishable latitudinal positions and a

split-like pattern (Fig. 7d–g). Two of them (Fig. 7d, e) retain the major features of the C3 and N3 clusters, and will be termed C4 and N4, keeping in mind the aforementioned discrepancies with the pure latitudinal regimes. They still concentrate EDJs occurring in the central and northern peaks, respectively, therefore preserving their distinctive features (e.g., weak intensity and eastern confinement for N4 and strong intensity and near-normal tilts for C4). The other two new clusters (Fig. 7f, g) come to a large extent from the S3 cluster, and span EDJs at latitudes ranging from the southern flank of the central peak to the southernmost positions. The first partition (Fig. 7f) corresponds to southward-shifted EDJs with large tilts (St4, hereafter), reflecting the variation of C EDJs with characteristics similar to S EDJs (i.e., a preference for weak EDJs with western locations; Fig. 6g). The second one (Fig. 7g) shares similarities with the mixed pattern in Madonna et al. (2017), and will be referred to as the split cluster (Sp4). The Sp4 cluster captures the characteristic two branches of split flows, which are not present in St4 EDJs. This suggests that a substantial fraction of S EDJs, particularly those located at the southernmost latitudes, correspond to split-like patterns with southern branches that eventually extend longitudinally and merge with the subtropical jet (Madonna et al. 2019). Despite sharing a preference for southern locations, the Sp4 and St4 clusters are distinguished by their intensity, longitudinal extension and zonal asymmetries, which often display opposite anomalies (not shown). Recent studies based on 2-D fields also needed four clusters to isolate EDJs of the southern peak (Madonna et al. 2017), or five clusters to separate the pervasive mixed pattern into split and tilted configurations (Dorrington and Strommen 2020). Thus, the choice of multi-parametric  $k=4$  multi-parametric clusters is a good compromise to describe preferred configurations of the NATL EDJ without losing the latitudinal perspective and will be used in the rest of this section.

Two remarks about the multi-parametric clusters should be made before continuing. First, for the analyses presented here we obtain similar structures when different combinations of EDJ parameters are clustered, even if the selected subset is reduced to a few metrics. However, the resulting clusters can depend on the specific choice of EDJ parameters. In particular, *Lat* alone cannot reproduce the multi-parametric clusters (not shown), confirming the added value of the remaining EDJ parameters. Secondly, we also obtain reasonably similar spatial patterns to those of Fig. 7d–g when the clustering is applied to area-weighted anomalies of the low-pass filtered 2D zonal wind (Figure S2d–g). Therefore, the selected parameters are, to some extent, able to reconstruct spatially-resolved configurations of the EDJ. Based on this correspondence and the large variability of the EDJ on interannual and decadal time scales, the multi-parametric clusters may depend on the specific analyzed period, as also

reported for the 2D zonal wind (e.g. Dorrington and Strommen 2020). In spite of this, the multi-parametric approach has the additional advantage of yielding quantifiable metrics of relevant aspects of the EDJ that are not directly inferred from 2D fields, therefore providing further insights on the evolving nature of EDJs.

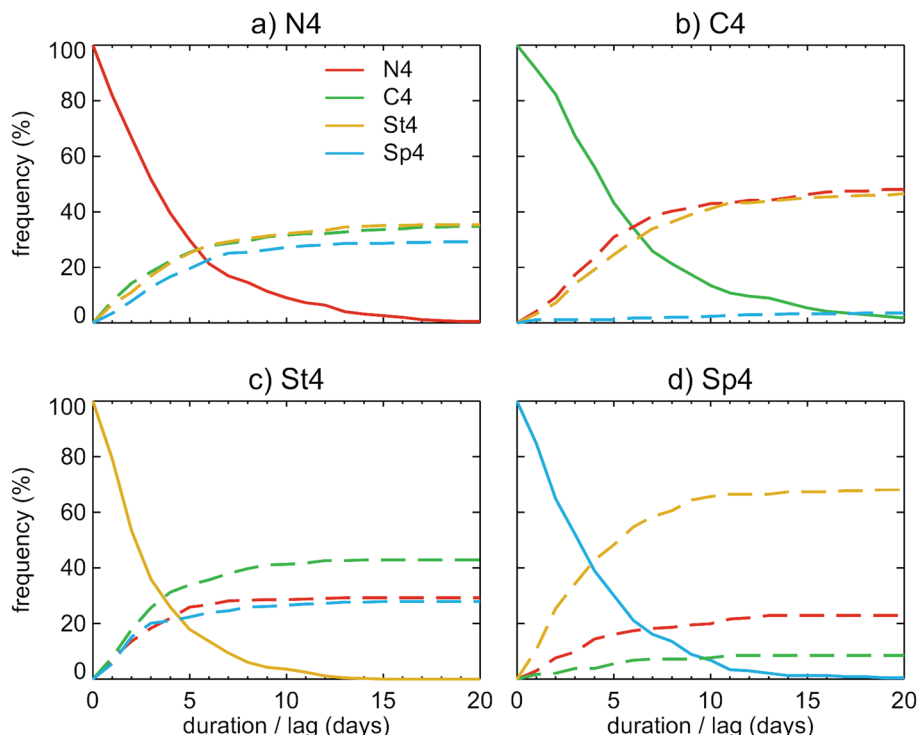
#### 4.4 Transitions between EDJ events

Here we explore the persistence and transitions of the four EDJ configurations that we have defined in the previous section. For each cluster  $k_i$ , we identify events, defined as one or more consecutive days classified in that cluster. Persistence is assessed by exploring the frequency distribution of  $k_i$  events with durations equal or longer than  $d$  days. To investigate the transitions of the  $k_i$  events, we use lags, with lag 0 denoting the first day of the event. For each lag, we count the fraction of  $k_i$  events that occupy a new cluster  $k_j$ . For long enough lags, all events will have transitioned to other states, and the cumulative frequency of  $k_j$  events accounts for the preferred transitions.

Figure 8 shows the distribution of event duration for each cluster and the cumulative occupancy of new states for lags up to 20 days. C4 is the most persistent state (Fig. 8b; 6.2 days), with higher autocorrelation coefficients and e-folding times than the other three clusters. Although N4 events have significantly low durations (4.7 days; Fig. 8a), as in previous studies (Barnes et al. 2010; Hannachi et al. 2012), they do not represent the least persistent state, since Sp4 and St4 events display comparable and even lower mean durations (smaller than 4.5 days; Fig. 8c, d). As for transitions, the events with the largest occupancies confirm the preferred poleward migration of EDJs (e.g., Franzke et al. 2011) from Sp4 to St4 (~69%, Fig. 8d), St4 to C4 (~43%; Fig. 8c) and C4 to N4 (~48%; Fig. 8b), although C4 events can also transition to nearby equatorward locations (St4) with high probability. Regarding migrations from N4 states (Fig. 8a), they are more likely followed by St4 events (35%), but the occupancy of these events is comparable to that of C4. Although likely, N4 migrations to the southern latitudinal peak (Sp4) show the lowest probability. Therefore, when more scrutinized EDJ patterns are considered, the reported abrupt transition of EDJs from the northern to the southern peak (Franzke et al. 2011; Hannachi et al. 2012) is not the preferred one, and N4 EDJs can more likely retrograde to C4 events or experience moderate latitudinal jumps to St4 states.

The transition paths inferred from the cumulative frequency of new events are consistent with the probabilities obtained from the transition matrix of a Markovian process, which defines the daily probability of moving from one cluster to another (e.g., Frame et al. 2011):

**Fig. 8** Frequency distribution with the number of EDJ events (solid lines) and cumulative transitions (dashed lines) as a function of the duration. Results are shown for the events defined from: **a–d** four (N4, C4, St4 and Sp4 events) multi-parametric clusters of the NATL EDJ. Frequencies are expressed in percentage of the total number of events in each cluster



$$P_{ij} = P(x_t \in k_j | x_{t-1} \in k_i) = P(x_t \in k_j, x_{t-1} \in k_i) / P(x_{t-1} \in k_i)$$

where  $P_{ij}$  is the probability of transitioning from  $k_i$  to  $k_j$  at any lag  $x_t$ . If we only consider transitions to another cluster by neglecting dates when the system stays in the same state (i.e., with zero diagonal terms; Franzke et al. 2011), the transition matrix is:

$$P = \begin{bmatrix} 0.00 & 0.28 & 0.03 & 0.30 \\ 0.69 & 0.00 & 0.48 & 0.35 \\ 0.09 & 0.42 & 0.00 & 0.35 \\ 0.22 & 0.29 & 0.49 & 0.00 \end{bmatrix}$$

$$\equiv \begin{bmatrix} & \text{St} \rightarrow \text{Sp} & \text{C} \rightarrow \text{Sp} & \text{N} \rightarrow \text{Sp} \\ \text{Sp} \rightarrow \text{St} & & \text{C} \rightarrow \text{St} & \text{N} \rightarrow \text{St} \\ \text{Sp} \rightarrow \text{C} & \text{St} \rightarrow \text{C} & & \text{N} \rightarrow \text{C} \\ \text{Sp} \rightarrow \text{N} & \text{St} \rightarrow \text{N} & \text{C} \rightarrow \text{N} & \end{bmatrix}$$

The most likely and unlikely transitions are denoted in bold and italics, respectively, if the probability is significantly ( $p < 0.05$ ) different from that expected from equally likely transitions (binomial test). In agreement with the poleward migration, Sp4 events show a strong preference to transition to St4, and St4 EDJs are indeed more likely to move poleward (C4) than equatorward (Sp4). The short duration of Sp4 and St4 states and the high probability of transitions between them explain why they tend to be merged under the same cluster in  $k = 3$ . These states could then be viewed as transitional phases between N4 and C4 EDJs. When considered together, we recover the preferred

loop S–C–N–S of transitions between the three latitudinal regimes (Franzke et al. 2011). However, from a deeper multi-parametric perspective, EDJs events simply reveal increasing transition probabilities towards their closest latitudinal states.

The transitions just described can be better explored by examining composites of EDJ parameters for selected transitions between events of at least 4-day durations (i.e., periods of four or more consecutive days in the cluster  $k_i$  followed by at least four consecutive days in the new regime  $k_j$ ) (Fig. 9). For the selected transitions (the poleward migration Sp4–St4–C4–N4), lagged composites of EDJ parameters have been computed with respect to the onset (lag 0) of the new event. Overall, shifts between EDJs at nearby latitudinal positions are associated with small tendencies of EDJ parameters, more pronounced for small negative lags. For example, St4–C4 and C4–N4 transitions show increasing tendencies of *Lat* and *Lon*, denoting an eastward progression of EDJs as they move poleward (Fig. 9b, c). In addition, EDJs tend to become more intense, zonally symmetric (negative tendencies of *Dep*), and with a lower *Til* when they move from St4 to C4 states, whereas the opposite evolution is observed for additional poleward shifts (from C4 to N4). Despite involving similar changes in latitude, Sp4–St4 transitions (Fig. 9a) show larger changes than the other ones involved in the poleward migration, including pronounced increases in *Til* and reduced *Dep*.

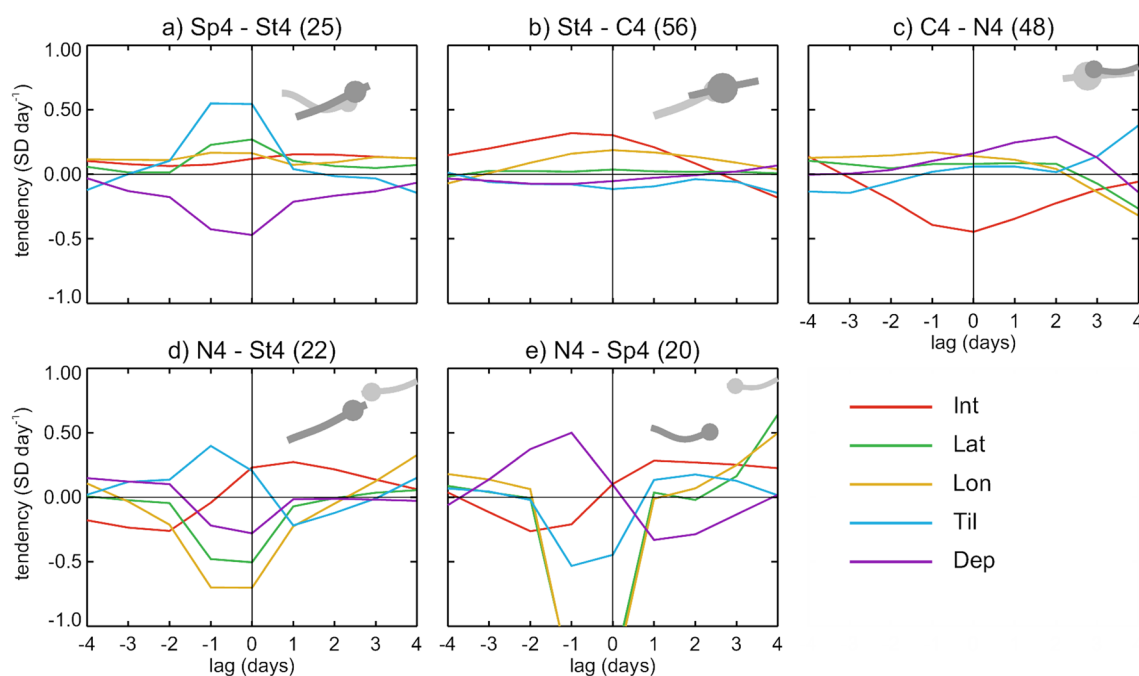


**Fig. 9** Composite tendency of EDJ parameters (in  $\text{SD day}^{-1}$ ) during the preferred transitions of EDJ events, as defined from the four multi-parametric clusters of the NATL EDJ: **a** Sp4 to St4; **b** St4 to C4; **c** C4 to N4; **d** N4 to St4; **e** N4 to Sp4 transitions. Lag 0 corresponds to the first day of the transitioned event. Only events of at

least four days are considered. The number of transitions considered for the composites are shown in brackets in the title. Snake-plots in the top right of each panel show the composited EDJ structure before (lag -3, light grey) and after (lag 3, dark grey) the transition

To further highlight the differences between Sp4 and St4 events, we compare transitions from N4 EDJs to these states. N4-Sp4 transitions (Fig. 9e) are characterized by increases in *Dep* and decreases in *Til*, denoting a split of tilted N4 EDJs into two separate branches. The southern one dominates the zonal average after the transition, as revealed by the large drop in *Lat*, giving rise to the characteristic features of Sp4 EDJs (weak intensity, small or negative tilts and a strong confinement to the western NATL). Differently, the comparatively more frequent N4-St4 transition (Fig. 9d) displays opposite tendencies to those of N4-Sp4, and smaller changes in *Dep* and in *Til*, with no split, but a reinforcement or extension of N4 EDJs towards the southeast in a highly tilted structure. During the transition, the entrance region of the tilted EDJ intensifies as the exit region weakens, so that the EDJ contracts to the southwest (large drop in *Lat* and *Lon*) and ends up as a St4 EDJ with reminiscent signatures of the original tilted configuration. Therefore, the intensification of winds at the entrance region of highly-tilted EDJs can be viewed as an abrupt equatorward transition from the latitudinal regime perspective.

## 5 Near-surface impacts of the EDJ

So far, we have shown that a reduced multi-parametric space provides a satisfactory description of the 2D EDJ variability, preferred states and transitions, as well as a manageable treatment of its complex structure. The latter is particularly useful to assess anomalous regional events and extreme events, which are expected to involve unusual EDJ parameters and configurations that match poorly with the canonical patterns described above. In this section, we move from the description of the EDJ to its associated impacts, which require considering single and combined effects of the EDJ parameters. The assessment of regional impacts of the EDJ on surface conditions of Europe has been typically done based on the latitudinal position (Mahlstein et al. 2012) and/or intensity of the zonal flow (e.g., Trigo et al. 2004). While these two parameters summarize the main modes of variability of the EDJ (shifting and pulsing), the associated impacts of other EDJ parameters remain unexplored. Here we illustrate two examples that highlight the added value of considering additional attributes of the EDJ to inform on regional climates.

We start showing that unexplored aspects of the EDJ can play a non-negligible influence on the well-reported

impacts of the EDJ latitude. To assess the effect of additional EDJ arrangements of the same latitudinal regime, composites of the zonal wind and 2-m temperature anomalies for the three latitudinal regimes have been further conditioned on a second EDJ parameter. As an illustrative example, Fig. 10 shows the *Til*-conditioned composites for each latitudinal regime. Panels of the same column correspond to EDJs of the same latitudinal regime, but with very different tilts, defined according to the lower and upper terciles of the *Til* distribution. Despite the tendency for C EDJs to be more tilted than S EDJs, we still identify a non-negligible frequency of occurrence of tilted S EDJs as well as C EDJs with negative tilts. For N regimes, the tilt is even less constrained, as shown by the similar frequencies of N EDJs with tilts in the upper and lower tercile of the distribution (see also Fig. 5b). The results indicate that the same latitudinal regime can be associated with very different (and frequently opposite) temperature anomalies depending on the tilt. Indeed, changes in temperature patterns tend to be larger between the tilt categories of the same latitudinal regime than across regimes. A similar behavior is observed for other surface variables

(e.g. precipitation) or if latitudinal regimes are conditioned on other EDJ parameters (not shown).

The variability of EDJ configurations and associated impacts within the same latitudinal regime means that latitude alone provides incomplete information of near-surface fingerprints of the EDJ. To deep into this issue, we exploit the multi-parametric approach and consider all EDJ parameters in order to identify those that account for the highest variance of near-surface fields at each grid point of Europe. To do so, we perform a multilinear regression of monthly variables (detrended 2-m temperature and precipitation anomalies) against the monthly mean EDJ parameters (Fig. 11). To account for co-linearity among the predictors, a stepwise approach has been adopted (Wilks 2006), which performs a forward selection with backward elimination, in order to retain only the predictors that increase significantly the amount of explained variance of the predictand. The amount of explained variance by the regression model is considerable (Fig. 11a, d; locally exceeding 50%), considering the local nature of the predictand and the large-scale character of the predictors. As expected, the influence of the EDJ parameters on near-surface variables tends to be larger

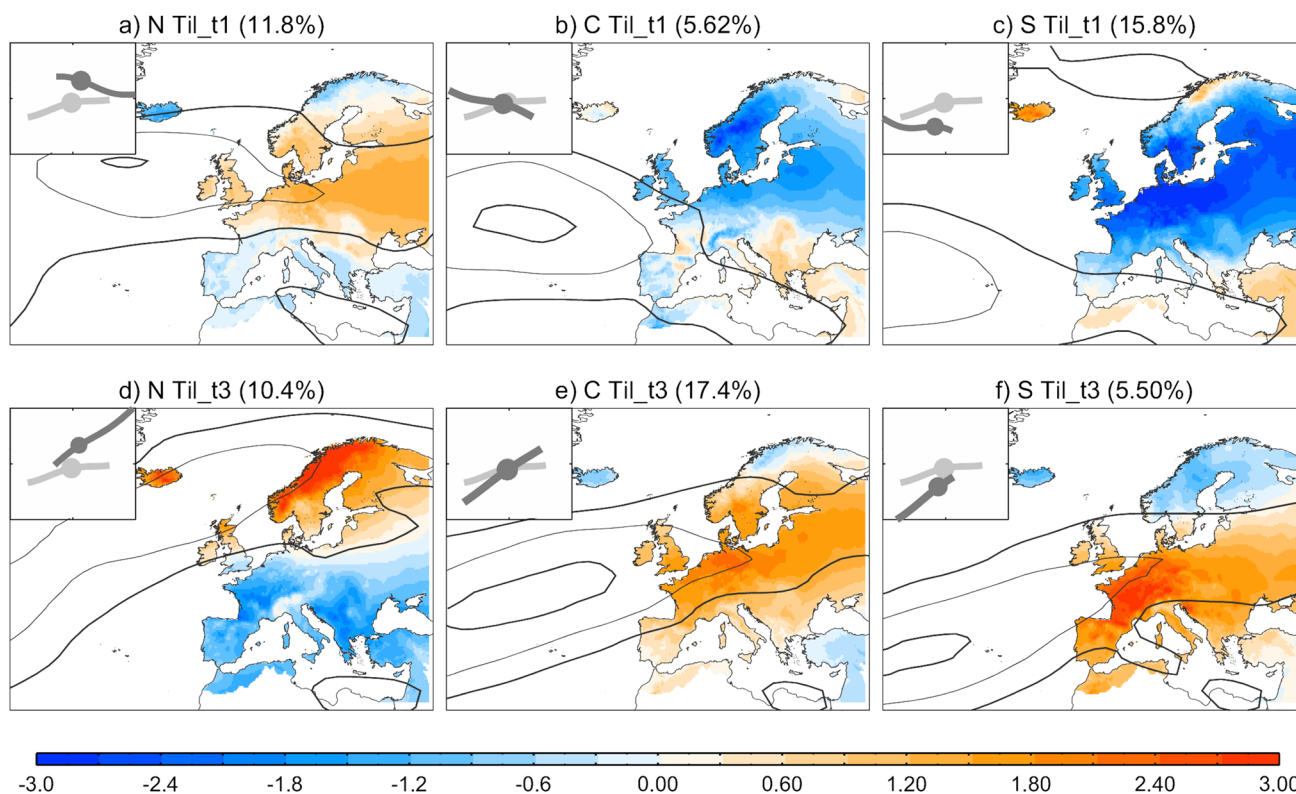


**Fig. 10** Composites of zonal wind at 925–700 hPa (contours, with contour interval of 5 m s<sup>-1</sup> starting at 5 m s<sup>-1</sup>) and 2 m temperature anomalies (shading, °C) for EDJs of the three latitudinal regimes with: **a–c** low (lower tercile, t1); **d–f** high (upper tercile, t3) tilts. Panel columns represent the northern (N, **a, d**), central (C, **b, e**) and

southern (**c, f**) EDJ regimes. The inset of each panel represents snakeplots of the EDJ for the climatology (light grey) and the composite (dark grey). The percentage of winter days included in the composite is shown in the title

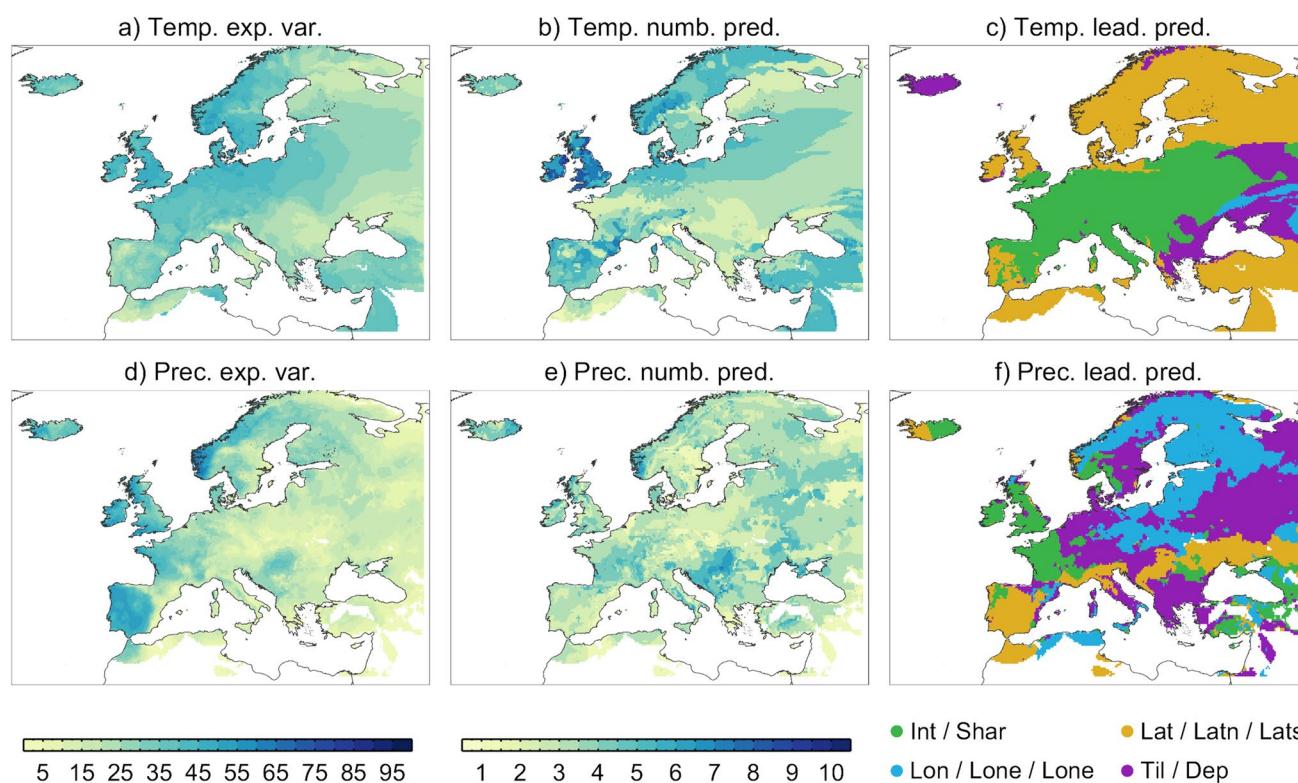


**Fig. 11** Stepwise regression model (1950–2020) of monthly temperature (a–c) and precipitation (d–f) onto the NATL EDJ parameters: **a, d** Percentage of variance of 2 m temperature (a) and precipitation (d) explained by the EDJ parameters (contour interval of 5%, following the numbers without parentheses in the color bar); **b, e** number of EDJ parameters selected as predictors of 2 m temperature (b) and precipitation (d) anomalies by the stepwise regression model (the

scale is given in parentheses in the color bar); **c, f** the best EDJ predictor of 2 m temperature (c) and precipitation (d) anomalies. Colors represent the groups of EDJ parameters: strength (green), latitudinal (yellow), longitudinal (blue) and zonal asymmetry (purple) parameters. White areas denote regions where none of the predictors can explain a significant amount of variance

over western than eastern Europe. On the other hand, the stepwise regression identifies at least one, but more commonly several EDJ parameters associated with monthly fluctuations of temperature and precipitation across Europe (Fig. 11b, e). There are no obvious links between the number of selected predictors and the amount of explained variance: high explained variances do not necessarily involve a larger number of skillful predictors, and vice versa.

To summarize the regions where each EDJ parameter has the strongest influence, we show the leading predictor of the local regressions (Fig. 11c, f). For readability, EDJ parameters have been grouped into four categories, related to wind speed (*Int*, *Shar*), zonal asymmetries (*Til*, *Dep*), and latitudinal (*Lat*, *Latn*, *Lats*) and longitudinal (*Lon*, *Lone*, *Lonw*) aspects of the EDJ. The results reveal a spatial heterogeneity of leading EDJ parameters, which is more pronounced in the case of precipitation. Speed-related parameters tend to dominate temperature

and precipitation fluctuations over western and some central European regions. Latitudinal parameters of the EDJ are the most important drivers of winter temperature anomalies over northern and southern Europe, as well as of precipitation anomalies in some regions of southern Europe. Longitudinal and zonal asymmetry parameters are the leading predictors in eastern Europe, and encompass large areas in the case of precipitation, although with low explained variances. Overall, these patterns agree with previous studies reporting the importance of wind speed and direction in modulating temperature and precipitation anomalies across Europe through horizontal temperature advection and humidity fluxes, respectively (e.g. Barriopedro et al. 2014, and references therein). They also stress the importance of considering the multi-faceted nature of the EDJ instead of focusing on a single parameter to explore the effects of EDJ configurations on European near-surface weather and climate.

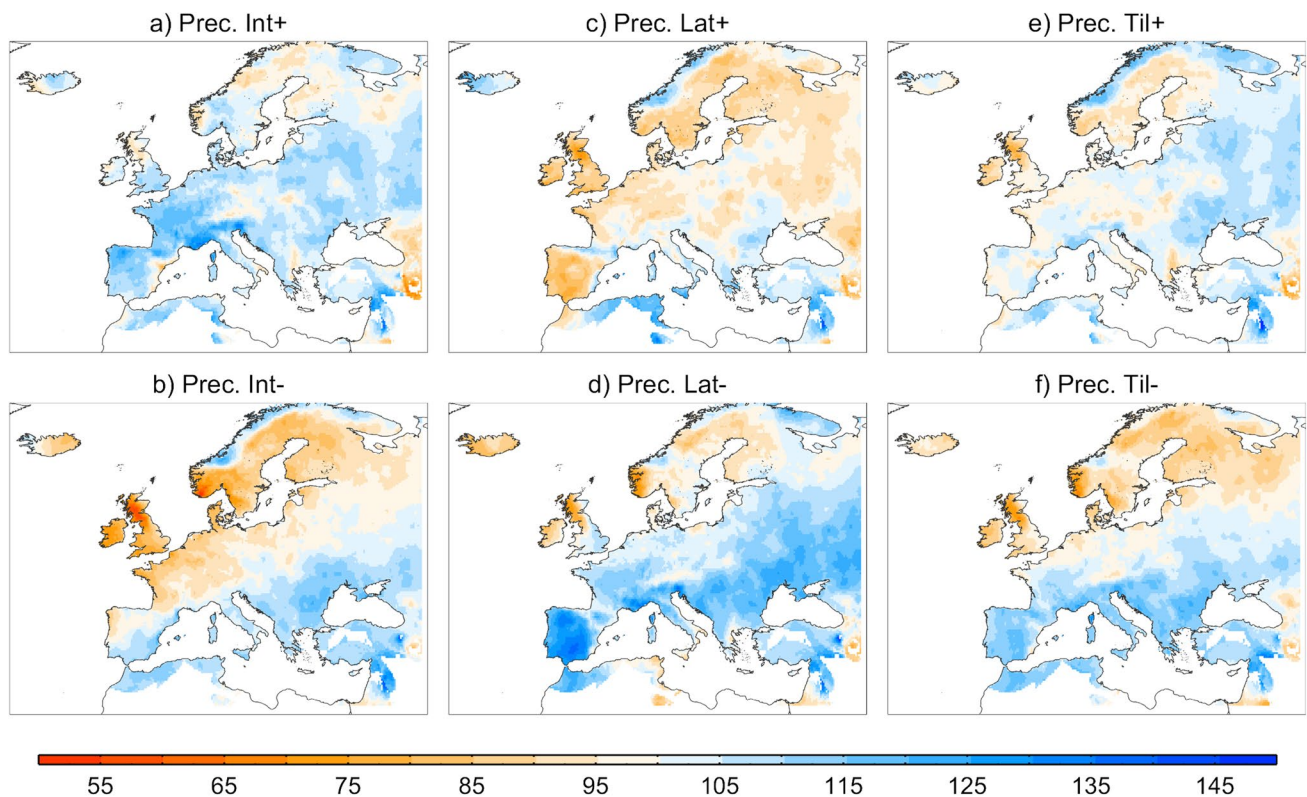


**Fig. 12** Monthly precipitation anomalies (in percentage of normals) reconstructed with a multilinear regression model based on selected parameters of the NATL EDJ (intensity, latitude, tilt and latitudinal width). Panels show the expected precipitation responses for the same narrowing of the EDJ ( $-1$  SD) and half changes of opposite sign

( $\pm 0.5$  SD, rows) in one of the other EDJ parameters (columns): **a, b** intensity; **c, d** latitude; **e, f** tilt, with plus and minus symbols in the title denoting positive ( $+0.5$  SD, **a, c, e**) and negative ( $-0.5$  SD, **b, d, f**) changes, respectively

## 6 Conclusions and discussion

In this study, we present a new suite of daily parameters of the North Atlantic (NATL) eddy-driven jet (EDJ) based on low-tropospheric (925–700 hPa) zonal wind data of the NCEP/NCAR reanalysis for the 1948–2020 period. The method represents a natural extension of a consolidated methodology for the characterization of the three latitudinal regimes of the NATL EDJ (e.g., Woollings et al. 2010), but covers additional salient features of the EDJ. The parameters correspond to the intensity and sharpness, position, including the latitudinal boundaries and eastward and westward extensions, as well as aspects related to zonal asymmetries, therefore accounting for multi-variate configurations of the NATL EDJ. Along with the daily parameters, we also provide a 2D identification of the EDJ based on regional means of zonal wind computed through the NATL, which yields a more traceable description of the EDJ structure and its spatial variations. The main conclusions are summarized as follows:

- *A novel multi-parametric perspective of the EDJ.* The new multi-parametric perspective of the EDJ presents several advantages. First, the EDJ parameters are based on regional aspects of the basic zonal flow, being robust to the spatial resolution of the data and minimizing local influences. The selected metrics focus on specific characteristics of the regional mean wind maxima that define the NATL EDJ, and dissect its structure beyond the classical latitudinal description. Synthesizing the EDJ structure in a manageable number of relevant aspects allows one to address complex or unusual EDJ configurations in a more tractable way than that of high-dimensional approaches. The EDJ parameters also avoid the use of subjective choices (thresholds and anomalies), and this enables the direct application of the methodology to other reanalysis datasets as well as model simulations with different climate realms, offering a wide range of applications (e.g., past climate studies, model evaluation, projections under different climate change scenarios, etc.). Finally, the proposed metrics are a good choice when daily time series of specific features of the EDJ are desired. One limitation of this approach can be the rela-

tively large number of defined parameters and the complexity of managing them altogether. However, although we provide a complete catalogue of relevant EDJ metrics, a scrutinized selection of parameters or tailored single-parameter assessments can be made depending on the specific aspects of the EDJ one is interested. As such, the EDJ parameters can be used in isolation or in combination, although the latter requires caution since some of them are not independent by construction.

- *Improved characterization of the EDJ.* The trimodality of the EDJ is intrinsic to latitude, since we do not identify a similar behavior in any other aspect of the EDJ, not even in its latitudinal margins. However, it has an effect on the longitudinal position of the EDJ, with a tendency for an eastern confinement of poleward EDJs, and more preferred western locations of southern EDJs. The results support previous studies regarding the influence of physical features such as orography, coastlines or ocean currents on the position of the NATL EDJ (Woollings et al. 2010; White et al. 2019). On seasonal scales, the tilt of the EDJ also tends to increase with latitude, but this relationship is not so evident on daily scales, which could explain some controversial results found in the literature. On the other hand, the reduced daily variability of the EDJ as it strengthens (Woollings et al. 2018) applies to parameters other than latitude and seems to reflect a general property of the EDJ.
- *Better understanding of the EDJ variability and dynamical forcing.* Variations in the EDJ parameters tend to have distinctive patterns in eddy forcing and wave breaking, which provides some dynamical background to the multi-parametric classification of EDJs. While both types of wave breaking are involved in pulsing and shifting of the EDJ, other variations of the EDJ, such as zonal asymmetries are strongly mediated by AWB. Different aspects of the zonally asymmetric EDJ structure are linked to different regions of anomalous AWB occurrence, and hence the specific location of AWB may play an important role in determining the future configuration of the EDJ. This is relevant because disturbed EDJs linked to these zonal asymmetries represent regions of the EDJ space for which the predictability decreases (Frame et al. 2013).
- *A synthesized view of recurrent EDJ configurations and transitions.* The same latitudinal regime can exhibit substantial departures from its canonical pattern and hide more complex structures that the latitude is unable to scrutinize. Therefore, a combination of several parameters is required to represent the 2D EDJ structure and its variability. The assessment of the multi-parametric space of the EDJ confirms some preferred states, but also a large spread of EDJ parameters combinations. The multi-parametric states of the EDJ capture well the

preferred patterns inferred from the full 2-D zonal wind. Consistent with previous studies on Euro-Atlantic flow regimes (e.g., Cassou et al. 2004), we find that a more satisfactory description of 2D EDJ patterns is reached when four multi-parametric clusters are considered. They correspond to northern (N4) and central (C4) EDJs, a southward-shifted tilted configuration (St4) and a split-like (Sp4) pattern concentrating the southernmost latitudes of the EDJ. The two latter are undistinguishable in the three latitudinal perspective, and this could explain the high persistence of the southern regime as compared to the central undisturbed state (Franzke et al. 2011; Hannachi et al. 2012). The four clusters show some tendency for a poleward migration of EDJs (Sp4-St4-C4-N4 events), which is further accompanied by an eastward progression, followed by a weakening and increasing asymmetry as the EDJ approaches the northern state. The abrupt jump from northern to southern latitudes reported in previous studies is not that likely when tilted and split EDJ patterns are distinguished by the multi-parametric lens.

- *Improved characterization of EDJ impacts on surface climate.* The multi-parametric perspective of the EDJ is also eminently useful for the assessment of regional climate conditions and their links with the large-scale circulation. Different EDJ configurations within the same latitudinal regime can cause substantially different (even opposite) impacts and hence the EDJ latitude alone conveys limited information of the surface responses to the EDJ. This is because the variability of near-surface variables such as 2-m temperature and precipitation is modulated by a combination of EDJ parameters, and in many regions the latitude does not turn up as the main predictor. It follows that changes in individual aspects of the EDJ can have additive or counteracting effects in surface climate conditions. This has implications for the dynamical assessment of extreme events, which may be associated with specific combinations of EDJ parameters.

Finally, the multi-parametric approach also offers promising prospects for the investigation of future regional climates. Recent studies have reported large uncertainties in future projections of the EDJ (e.g., Barnes and Polvani 2013; Zappa and Shepherd 2017; Peings et al. 2018). A substantial part of this uncertainty arises from (but is not limited to) competing influences of the projected Arctic Amplification and Tropical Warming on the EDJ latitude (e.g., Peings et al. 2018; Oudar et al. 2020; Lee et al. 2021). There is some consensus that this tug-of-war would promote a narrowing of the EDJ, albeit with considerable uncertainty in other EDJ aspects. To illustrate the different responses of precipitation to changes in these uncertain parameters under the same squeezing

of the EDJ, we have constructed a multilinear regression model using detrended monthly mean series (1950–2020) of the precipitation and selected EDJ parameters (*Int*, *Lat* and *Til* and the width of the EDJ, *Wid*, defined as the difference between poleward and equatorward boundaries of the EDJ). Figure 12 shows the precipitation anomalies reconstructed for a large narrowing of the EDJ ( $-1$  SD in *Wid*) and imposing moderate changes ( $\pm 0.5$  SD) in one of the other EDJ parameters.

Overall, we find a large spread of precipitation responses to the same change in the EDJ width, depending on changes in other EDJ parameters. For some regions (e.g. Iberia or northwestern Europe), the responses are ruled by the “uncertainty” in a given parameter rather than by the “robust” squeezing of the EDJ. One may assume that some scenarios are more likely to occur than others in response to an EDJ narrowing (e.g., EDJ intensification and increased zonality). However, for these cases, the recovered spatial patterns (Fig. 12a, f) are still very different, eventually involving opposite regional responses (e.g., over Scandinavia). Although this analysis is only used for illustrative purposes and should not be extrapolated to future conditions, it suggests that even if projections of the EDJ width were robust across models, the uncertainty in other EDJ parameters could prevent a clear picture of EDJ-induced changes in regional climates. The multi-parametric diagnosis of the EDJ adopted here provides a useful tool to explore plausible forced changes in the complex EDJ structure as simulated by multi-model ensembles of future projections, as well as their associated impacts in regional climates.

**Supplementary Information** The online version contains supplementary material available at <https://doi.org/10.1007/s00382-022-06574-w>.

**Acknowledgements** This research is part of the CSIC Interdisciplinary Thematic Platform (PTI) Clima y Servicios Climáticos (PTI-CLIMA) and POLARCSIC (PTI-POLAR) activities. The valuable comments of two anonymous reviewers helped to improve the manuscript.

**Author contributions** All authors contributed to the study conception and design. Material preparation, data collection and analysis were performed by DB. The first draft of the manuscript was written by DB and all authors contributed to improve it through comments and changes in the text, structure and content. All authors approved the final manuscript.

**Funding** Open Access funding provided thanks to the CRUE-CSIC agreement with Springer Nature. This work was supported by the Spanish Ministerio de Ciencia, Innovación y Universidades through the JeDiS (RTI2018-096402-B-I00) project. MGB was also supported by the Spanish Ministerio de Ciencia e Innovación (Grant PRE2019-090618).

**Data availability** Datasets used in this study is publicly accessible online via the following links: NCEP/NCAR dataset: <https://psl.noaa.gov/data/gridded/data.ncep.reanalysis.html>. E-OBS dataset: [https://surfobs.climate.copernicus.eu/dataaccess/access\\_eobs\\_months.php](https://surfobs.climate.copernicus.eu/dataaccess/access_eobs_months.php).

ERA5 dataset: <https://www.ecmwf.int/en/forecasts/datasets/reanalysis-datasets/era5>. The EDJ datasets generated during the current study are available from the corresponding author upon request.

## Declarations

**Conflict of interest** The authors have no relevant financial or non-financial interests to disclose.

**Open Access** This article is licensed under a Creative Commons Attribution 4.0 International License, which permits use, sharing, adaptation, distribution and reproduction in any medium or format, as long as you give appropriate credit to the original author(s) and the source, provide a link to the Creative Commons licence, and indicate if changes were made. The images or other third party material in this article are included in the article's Creative Commons licence, unless indicated otherwise in a credit line to the material. If material is not included in the article's Creative Commons licence and your intended use is not permitted by statutory regulation or exceeds the permitted use, you will need to obtain permission directly from the copyright holder. To view a copy of this licence, visit <http://creativecommons.org/licenses/by/4.0/>.

## References

- Athanasiadis PJ, Wallace JM, Wettstein JJ (2010) Patterns of wintertime jet stream variability and their relation to the storm tracks. *J Atmos Sci* 67:1361–1381
- Barnes EA, Hartmann DL (2010) Dynamical feedbacks and the persistence of the NAO. *J Atmos Sci* 67:851–865
- Barnes EA, Hartmann DL (2011) Rossby wave scales, propagation, and the variability of eddy-driven jets. *J Atmos Sci* 68:2893–2908
- Barnes EA, Polvani LM (2013) Response of the midlatitude jets, and of their variability, to increased greenhouse gases in the CMIP5 models. *J Clim* 26:7117–7135
- Barnes EA, Hartmann DL, Frierson DMW, Kidston J (2010) Effect of latitude on the persistence of eddy-driven jets. *Geophys Res Lett* 37:L11804. <https://doi.org/10.1029/2010GL043199>
- Barriopedro D, Gallego D, Alvarez-Castro MC, Garcia-Herrera R, Wheeler D, Peña-Ortiz C, Barbosa SM (2014) Witnessing North Atlantic westerlies variability from ships' logbooks (1685–2008). *Clim Dyn* 43:939–955. <https://doi.org/10.1007/s00382-013-1957-8>
- Benedict JJ, Lee S, Feldstein SB (2004) Synoptic view of the North Atlantic oscillation. *J Atmos Sci* 61:121–144
- Blackmon ML (1976) A climatological spectral study of the 500 mb geopotential height of the Northern Hemisphere. *J Atmos Sci* 33:1607–1623
- Cassou C, Terray L, Hurrell JW, Deser C (2004) North American winter climate regimes: spatial asymmetry, stationarity with time, and oceanic forcing. *J Clim* 17:1055–1068
- Cattiaux J, Peings Y, Saint-Martin D, Trou-Kechout N, Vavrus SJ (2016) Sinuosity of midlatitude atmospheric flow in a warming world. *Geophys Res Lett* 43:8259–8268. <https://doi.org/10.1002/2016GL070309>
- Ceppi P, Zelinka MD, Hartmann DL (2014) The response of the Southern Hemispheric eddy-driven jet to future changes in shortwave radiation in CMIP5. *Geophys Res Lett* 41:3244–3250. <https://doi.org/10.1002/2014GL060043>
- Chen HW, Zhang F, Alley RB (2016) The robustness of midlatitude weather pattern changes due to Arctic Sea ice loss. *J Clim* 29:7831–7849

- Davini P, Cagnazzo C, Neale R, Tribbia J (2012) Coupling between Greenland blocking and the North Atlantic Oscillation pattern. *Geophys Res Lett* 39:L14701. <https://doi.org/10.1029/2012GL052315>
- Di Capua G, Coumou D (2016) Changes in meandering of the Northern Hemisphere circulation. *Environ Res Lett* 11:094028. <https://doi.org/10.1088/1748-9326/11/9/094028>
- Dorrington J, Strommen KJ (2020) Jet speed variability obscures Euro-Atlantic regime structure. *Geophys Res Lett* 47:e2020GL087907. <https://doi.org/10.1029/2020GL087907>
- Eichelberger SJ, Hartmann DL (2007) Zonal jet structure and the leading mode of variability. *J Clim* 20:5149–5163
- Frame THA, Ambaum MHP, Gray SL, Methven J (2011) Ensemble prediction of transitions of the North Atlantic eddy-driven jet. *Q J R Meteorol Soc* 137:1288–1297
- Frame THA, Methven J, Gray SL, Ambaum MHP (2013) Flow dependent predictability of the North Atlantic jet. *Geophys Res Lett* 40:2411–2416. <https://doi.org/10.1002/grl.50454>
- Franzke C, Woollings T (2011) On the persistence and predictability properties of North Atlantic climate variability. *J Clim* 24:466–472. <https://doi.org/10.1175/2010JCLI3739.1>
- Franzke C, Woollings T, Martius O (2011) Persistent circulation regimes and preferred regime transitions in the North Atlantic. *J Atmos Sci* 68:2809–2825
- García-Herrera R, Garrido-Perez JM, Barriopedro D, Ordoñez C, Vicente-Serrano SM, Nieto R, Gimeno L, Sorí R, Yiou P (2019) The European 2016/17 drought. *J Clim* 32:3169–3187
- Gerber EP, Vallis GK (2007) Eddy-zonal flow interactions and the persistence of the zonal index. *J Atmos Sci* 64:3296–3311
- Hannachi A, Woollings T, Fraedrich K (2012) The North Atlantic jet stream: a look at preferred positions, paths and transitions. *Q J R Meteorol Soc* 138:862–877. <https://doi.org/10.1002/qj.959>
- Haylock MR, Hofstra N, Klein Tank AMG, Klok EJ, Jones PD, New M (2008) A European daily high-resolution gridded data set of surface temperature and precipitation for 1950–2006. *J Geophys Res* 113:D20119. <https://doi.org/10.1029/2008JD010201>
- Held IM, Hou AY (1980) Nonlinear axially symmetric circulations in a nearly inviscid atmosphere. *J Atmos Sci* 37:515–533
- Hersbach H, Bell B, Berrisford P et al (2020) The ERA5 global reanalysis. *Q J R Meteorol Soc* 146:1999–2049. <https://doi.org/10.1002/qj.3803>
- Hoskins BJ, James IN, White GH (1983) The shape, propagation and mean-flow interaction of large-scale weather systems. *J Atmos Sci* 40:1595–1612
- Iqbal W, Leung WN, Hannachi A (2018) Analysis of the variability of the North Atlantic eddy-driven jet stream in CMIP5. *Clim Dyn* 51:235–247. <https://doi.org/10.1007/s00382-017-3917-1>
- Kalnay ME, Kanamitsu M, Kistler R et al (1996) The NCEP/NCAR 40-year reanalysis project. *Bull Am Meteorol Soc* 77:437–471
- Koch P, Wernli H, Davies HC (2006) An event-based jet stream climatology and typology. *Int J Climatol* 26:283–301
- Lee S, Son S-W, Grise K, Feldstein SB (2007) A mechanism for the poleward propagation of zonal mean flow anomalies. *J Atmos Sci* 64:849–868. <https://doi.org/10.1175/JAS3861.1>
- Lee JY, Marotzke J, Bala G et al (2021) Future Global Climate: Scenario-Based Projections and Near-Term Information. In: Masson-Delmotte V, Zhai P, Pirani A et al (eds) *Climate change 2021: the physical science basis. Contribution of working group I to the sixth assessment report of the intergovernmental panel on climate change*. Cambridge University Press (**in Press**)
- Li C, Wettstein JJ (2012) Thermally driven and eddy-driven jet variability in reanalysis. *J Clim* 25:1587–1596
- Limbach S, Schömer E, Wernli H (2012) Detection, tracking and event localization of jet stream features in 4D atmospheric data. *Geosci Model Dev* 5:457–470. <https://doi.org/10.5194/gmd-5-457-2012>
- Lorenz DJ, Hartmann DL (2001) Eddy–zonal flow feedback in the Southern Hemisphere. *J Atmos Sci* 58:3312–3327
- Lorenz DJ, Hartmann DL (2003) Eddy–zonal flow feedback in the Northern Hemisphere winter. *J Clim* 16:1212–1227
- Madonna E, Li C, Grams CM, Woollings T (2017) The link between eddy-driven jet variability and weather regimes in the North Atlantic-European sector. *Q J R Meteorol Soc* 143:2960–2972. <https://doi.org/10.1002/qj.3155>
- Madonna E, Li C, Wettstein JJ (2019) Suppressed eddy driving during southward excursions of the North Atlantic jet on synoptic to seasonal time scales. *Atmos Sci Lett* 20:1–11
- Mahlstein I, Martius O, Chevalier C, Ginsbourger D (2012) Changes in the odds of extreme events in the Atlantic basin depending on the position of the extratropical jet. *Geophys Res Lett* 39:L22805. <https://doi.org/10.1029/2012GL053993>
- Mak M, Cai M (1989) Local barotropic instability. *J Atmos Sci* 46:3289–3311
- Martius O, Schwierz C, Davies HC (2007) Breaking waves at the tropopause in the wintertime northern hemisphere: climatological analyses of the orientation and the theoretical LC1/2 classification. *J Atmos Sci* 64:2576–2592
- Masato G, Hoskins BJ, Woollings TJ (2012) Wave-breaking characteristics of midlatitude blocking. *Q J R Meteorol Soc* 138:1285–1296
- Mellado-Cano J, Barriopedro D, García-Herrera R, Trigo R, Hernández A (2019) Examining the North Atlantic Oscillation, East Atlantic Pattern, and jet variability since 1685. *J Clim* 32:6285–6298
- Messori G, Caballero R (2015) On double Rossby wave breaking in the North Atlantic. *J Geophys Res Atmos* 120:11129–11150. <https://doi.org/10.1002/2015JD023854>
- Michel C, Rivière G (2011) The link between Rossby wave breakings and weather regime transitions. *J Atmos Sci* 68:1730–1748
- Monahan AH, Fyfe JC (2006) On the nature of zonal jet EOFs. *J Clim* 19:6409–6424
- Novak L, Ambaum MHP, Tailleux R (2015) The lifecycle of the North Atlantic storm track. *J Atmos Sci* 72:821–833. <https://doi.org/10.1175/JAS-D-14-0082.1>
- Ordóñez C, Barriopedro D, García-Herrera R (2019) Role of the position of the North Atlantic jet in the variability and odds of extreme PM10 in Europe. *Atmos Environ* 210:35–46. <https://doi.org/10.1016/j.atmosenv.2019.04.045>
- Oudar T, Cattiaux J, Douville H (2020) Drivers of the Northern Extratropical eddy-driven jet change in CMIP5 and CMIP6 models. *Geophys Res Lett* 47:e2019GL086695. <https://doi.org/10.1029/2019gl086695>
- Peings Y, Cattiaux J, Vavrus SJ, Magnusdottir G (2018) Projected squeezing of the wintertime North-Atlantic jet. *Environ Res Lett* 13:074016
- Peña-Ortiz C, Gallego D, Ribera P, Ordonez P, Alvarez-Castro MDC (2013) Observed trends in the global jet stream characteristics during the second half of the 20th century. *J Geophys Res Atmos* 118:2702–2713
- Rivière G (2009) Effect of latitudinal variations in low-level baroclinicity on eddy life cycles and upper-tropospheric wave-breaking processes. *J Atmos Sci* 66:1569–1592
- Rivière G, Orlanski I (2007) Characteristics of the Atlantic storm-track eddy activity and its relation with the North Atlantic Oscillation. *J Atmos Sci* 64:241–266
- Santos JA, Woollings T, Pinto JG (2013) Are the winters 2010 and 2012 archetypes exhibiting extreme opposite behavior of the North Atlantic jet stream? *Mon Weather Rev* 141:3626–3640
- Sousa PM, Barriopedro D, García-Herrera R, Woollings T, Trigo RM (2021) A new combined detection algorithm for blocking and subtropical ridges. *J Clim* 34:7735–7758

- Spensberger C, Spengler T, Li C (2017) Upper tropospheric jet axis detection and application to the boreal winter 2013/2014. *Mon Weather Rev* 145:2363–2374. <https://doi.org/10.1175/MWR-D-16-0467.1>
- Strommen K (2020) Jet latitude regimes and the predictability of the North Atlantic Oscillation. *Q J R Meteorol Soc* 146:2368–2391. <https://doi.org/10.1002/qj.3796>
- Strong C, Davis RE (2008) Variability in the position and strength of winter jet stream cores related to Northern Hemisphere teleconnections. *J Clim* 21:584–592
- Strong C, Magnusdottir G (2008) Tropospheric Rossby wave breaking and the NAO/NAM. *J Atmos Sci* 65:2861–2876
- Thorncroft C, Hoskins BJ, McIntyre ME (1993) Two paradigms of baroclinic wave life cycle behaviour. *Q J R Meteorol Soc* 119:17–55
- Trigo RM, Trigo IF, DaCamara CC, Osborn TJ (2004) Climate impact of the European winter blocking episodes from the NCEP/NCAR Reanalyses. *Clim Dyn* 23:17–28. <https://doi.org/10.1007/s00382-004-0410-4>
- Vallis GK, Zurita-Gotor P, Cairn C, Kidston J (2014) Response of the large-scale structure of the atmosphere to global warming. *Q J R Meteorol Soc* 141:1479–1501. <https://doi.org/10.1002/qj.2456>
- White RH, Hilgenbrink C, Sheshadri A (2019) The importance of Greenland in setting the northern preferred position of the North Atlantic eddy-driven jet. *Geophys Res Lett* 46:14126–14134
- Wilks DS (2006) *Statistical methods in the atmospheric sciences*, 2nd edn. Academic Press, London
- Woollings T, Blackburn M (2012) The North Atlantic jet stream under climate change and its relation to the NAO and EA patterns. *J Clim* 25:886–902. <https://doi.org/10.1175/JCLI-D-11-00087.1>
- Woollings T, Hannachi A, Hoskins B (2010) The variability of the North Atlantic eddy-driven jet stream. *Q J R Meteorol Soc* 136:856–868
- Woollings T, Pinto JG, Santos JA (2011) Dynamical evolution of North Atlantic ridges and poleward jet stream displacements. *J Atmos Sci* 68:954–963. <https://doi.org/10.1175/2011JAS3661.1>
- Woollings T, Barnes E, Hoskins B, Kwon Y-O, Lee RW, Li C, Madonna E, McGraw M, Parker R, Rodrigues R, Spensberger C, Williams K (2018) Daily to decadal modulation of jet variability. *J Clim* 31:1297–1314
- Zappa G, Shepherd TG (2017) Storylines of atmospheric circulation change for European regional climate impact assessment. *J Clim* 30:6561–6577
- Zurita-Gotor P, Blanco-Fuentes J, Gerber EP (2014) The impact of baroclinic eddy feedback on the persistence of jet variability in the two-layer model. *J Atmos Sci* 71:410–429

**Publisher's Note** Springer Nature remains neutral with regard to jurisdictional claims in published maps and institutional affiliations.